

ANL-7115

ANL-7115

Argonne National Laboratory

REACTOR DEVELOPMENT PROGRAM

PROGRESS REPORT

October 1965

LEGAL NOTICE

This report was prepared as an account of Government sponsored work. Neither the United States, nor the Commission, nor any person acting on behalf of the Commission:

A. Makes any warranty or representation, expressed or implied, with respect to the accuracy, completeness, or usefulness of the information contained in this report, or that the use of any information, apparatus, method, or process disclosed in this report may not infringe privately owned rights; or

B. Assumes any liabilities with respect to the use of, or for damages resulting from the use of any information, apparatus, method, or process disclosed in this report.

As used in the above, "person acting on behalf of the Commission" includes any employee or contractor of the Commission, or employee of such contractor, to the extent that such employee or contractor of the Commission, or employee of such contractor prepares, disseminates, or provides access to, any information pursuant to his employment or contract with the Commission, or his employment with such contractor.

ARGONNE NATIONAL LABORATORY
9700 South Cass Avenue
Argonne, Illinois 60440

REACTOR DEVELOPMENT PROGRAM
PROGRESS REPORT

October 1965

Albert V. Crewe, Laboratory Director
Stephen Lawroski, Associate Laboratory Director

<u>Division</u>	<u>Director</u>
Chemical Engineering	R. C. Vogel
Idaho	M. Novick
Metallurgy	F. G. Foote
Reactor Engineering	L. J. Koch
Reactor Physics	R. Avery
Remote Control	R. C. Goertz

Report coordinated by
R. M. Adams and A. Glassner

Issued November 23, 1965

Operated by The University of Chicago
under
Contract W-31-109-eng-38
with the
U. S. Atomic Energy Commission

FOREWORD

The Reactor Development Program Progress Report, issued monthly, is intended to be a means of reporting those items of significant technical progress which have occurred in both the specific reactor projects and the general engineering research and development programs. The report is organized in a way which, it is hoped, gives the clearest, most logical overall view of progress. The budget classification is followed only in broad outline, and no attempt is made to report separately on each sub-activity number. Further, since the intent is to report only items of significant progress, not all activities are reported each month. In order to issue this report as soon as possible after the end of the month editorial work must necessarily be limited. Also, since this is an informal progress report, the results and data presented should be understood to be preliminary and subject to change unless otherwise stated.

The issuance of these reports is not intended to constitute publication in any sense of the word. Final results either will be submitted for publication in regular professional journals or will be published in the form of ANL topical reports.

The last six reports issued
in this series are:

April 1965	ANL-7045
May 1965	ANL-7046
June 1965	ANL-7071
July 1965	ANL-7082
August 1965	ANL-7090
September 1965	ANL-7105

REACTOR DEVELOPMENT PROGRAM

Highlights of Project Activities for October 1965

EBR-II

Operation of the reactor proceeded very satisfactorily this month. A scheduled run was started on October 13, completed on October 21, and another started on October 29. At month's end, seven experimental irradiation subassemblies and three special fuel subassemblies for measuring capture to fission ratios were being irradiated in the reactor.

Eleven fuel subassemblies were transferred to the Fuel Cycle Facility for surveillance measurements and reprocessing. Seven reprocessed fuel subassemblies were transferred back to the reactor. The reactor now contains 13 reprocessed subassemblies with fuel which had previously been irradiated to levels up to 1.1% burnup.

Surveillance measurements have shown that no fuel pins have exceeded set allowable limits for growth. There has been no evidence of failed elements.

ZPR-3

Assembly of the SEFOR mockup was started at the end of the month.

ZPPR

Studies of the gravel samples taken during the coring of the Gravel Gertie test structure are continuing with the work being performed by Colorado School of Mines Research Foundation, Inc., as subcontractor. They are also to examine the catenary support structure used during the test.

FARET

Preparation of material requested by the ACRS Subcommittee has been completed and incorporated into Supplement No. 2 to the Preliminary Safety Analysis Report on the Fast Reactor Test Facility (FARET). It is expected that this material will be reviewed at the next ACRS meeting scheduled for November 10, 1965.

AARR

One of five basic arrangements prepared for the AARR plant complex by the architect-engineer has been chosen for intensive further development as the principal Title I design. The selected arrangement leads to improved operating flexibility and construction economy without affecting the fundamental design and safety criteria.

Calculations have shown that introduction of a layer of either graphite or aluminum between the beryllium reflector and the pressure vessel wall will simultaneously reduce the heating in the vessel wall and increase the thermal-neutron flux at instrument locations outside the wall.

A preliminary stress analysis of the AARR pressure vessel has been carried out primarily to determine the minimum permissible spacing of horizontal experimental beam port openings in the vessel and thereby to fix the maximum feasible number of such ports which can be provided.

Plutonium Recycle Program (EBWR)

A major portion of the month was spent on plant improvement and fuel-handling activities.

The 22-assembly loading in the EBWR was rearranged in a more symmetric configuration. For the new configuration, the cold, unpoisoned, reactor was critical with all control rods fully withdrawn except the central rod which was at a height of 41 in. The reactivity worth of the remaining 7 in. of the central control rod was found to be 10^{-3} from measurement of its differential worth.

TABLE OF CONTENTS

	<u>Page</u>
I. LIQUID-METAL-COOLED REACTORS	1
A. EBR-II	1
1. Operations	1
2. Systems and Components	1
3. Reactor Improvements	3
4. Reactor Physics	7
5. Fuel Surveillance	9
6. Fuel Cycle Facility	10
B. FARET	11
1. General	11
2. Reactor Vessel	11
3. Seismic Analysis of Piping for Sodium	12
4. Cell Operating Handling Mockup	13
5. Shielding Windows	14
6. Penetration of Tank Cover for Cable Take-up	14
7. In-core Instrumentation	14
8. Fuel Assembly Sodium Flow Test Loop	15
9. Stress Analysis of Core Support	15
10. Reference Core-I Design	17
11. Safety Analysis	21
12. Fabrication Methods for Experimental FARET Fuel Elements	24
C. General Fast Reactor Physics	25
1. ZPR-3	25
2. ZPR-6	27
3. ZPR-9	29
4. ZPPR	30
D. General Fast Reactor Fuel Development	31
1. Metallic Fuels	31
2. Jacket Materials	33
3. Fabrication of EBR-II-type Irradiation Specimens	34
4. Production of Supplemental U-Fs Alloy Fuel Pins for EBR-II	34
5. Carbide Fuels	35
6. Development of Refractory-metal Alloys for Service in Oxygen-contaminated Sodium	36

TABLE OF CONTENTS

	<u>Page</u>
E. General Fast Reactor Fuel Reprocessing Development	37
1. Skull Reclamation Process	37
2. Processes for Future Fast Reactor Fuels	38
3. Materials Evaluation	40
II. GENERAL REACTOR TECHNOLOGY	42
A. Experimental Reactor and Nuclear Physics	42
1. Measurements of Small Reactivity in ATSR	42
2. High Conversion Critical Experiments (Hi-C)	44
B. Theoretical Reactor Physics	44
1. Effects of Randomness on Group Cross Sections	44
2. The Argonne Reactor Computation System (ARC)	45
3. Development of Reactor Computing Codes	48
4. Evaluation of Cross Sections	48
C. High-temperature Materials Studies	49
1. Ceramic Fuel Materials	49
2. Liquid-metal Corrosion	55
3. Irradiation of Materials for Fast Reactors	56
D. Other Reactor Fuels and Materials Development	60
1. Nondestructive Testing	60
E. Engineering Development	62
1. Two-phase Flow	62
2. Boiling Liquid-metal Technology	62
3. General Heat Transfer	63
F. Chemical Separations	64
1. Fluidization and Volatility Separations Processes	64
G. Sodium Coolant Chemistry	66
1. Control of Sodium Oxide Impurity	66

TABLE OF CONTENTS

	<u>Page</u>
H. Plutonium Recycle Program	66
1. Operations	66
2. Reactor Plant Preparation and Maintenance	66
III. ADVANCED SYSTEMS RESEARCH AND DEVELOPMENT	68
A. Argonne Advanced Research Reactor (AARR)	68
1. General	68
2. Theoretical Physics Analyses	69
3. Heat Transfer	71
4. Stress Studies of the Reactor Vessel	71
5. Primary System and Components	72
B. Very Large Fast Breeder Reactor for Desalination	74
C. Energy-conversion Systems	75
1. Regenerative Emf Cells	75
2. Bimetallic Cells	76
IV. NUCLEAR SAFETY	78
A. Reactor Kinetics	78
1. MTR Irradiations of UO_2 Specimens	78
2. Fast Reactor Safety	78
B. TREAT	79
1. Operations	79
2. Large TREAT Loop	80
C. Chemical and Associated Energy-transfer Problems in Reactor Safety	81
1. Metal-Water Reactions	81
V. PUBLICATIONS	84

I. LIQUID-METAL-COOLED REACTORS

A. EBR-II

1. Operations

The reactor was started up on October 13 following shutdown for fuel surveillance and some reloading. Stability parameters and power coefficients were measured during incremental power increases to 45 MW. Power operation was concluded on October 21 at 3,665 MWd(t) to limit the burnup in the Row 4 subassemblies to 1.2% maximum. Integrated reactor power for this run was 345 MWd(t). A total of 2,596 MWh of electricity was produced. The reactor was started up again on October 29 for the next increment of power operation.

A total of 10 experimental irradiation subassemblies were installed in the inner blanket and core region of the reactor during the October 13 run. One subassembly (A776X) containing special elements for the measurement of α by Argonne's Chemical Engineering Division was removed from the reactor, and one experimental irradiation subassembly (XA07) was installed.

2. Systems and Components

a. Reactor Building. Electrical penetrations Nos. 9, 10, 13, 29, 31, and 36 into the reactor building have been furnished with secondary flanges and connectors to enable their being leak-tested without disconnecting their contained circuits. Blind flanges were installed on penetrations 24, 25, and 27, which are spares and not in use. This arrangement will allow leak-testing of these penetrations and will give an indication of the development of leaks through the gasket material used on all penetrations. When the above penetrations were leak tested at 25 psig for 8 hr, all had leak rates of less than 0.013 cu ft/day corrected to 36.2 psig and 32°F. Therefore, all penetrations tested showed a leak rate less than that listed in the original construction specification requirements. These nine penetrations will be tested for leak rates annually.

b. Rotating Plug Seals. Prior to operation of the reactor, the power necessary to melt the seals of the rotating plugs was reduced. The lower heater-control temperature was reduced from 400 to 380°F, and the upper heater Variac settings were reduced from 90 to 60%. At these conditions, it was possible to rotate both seals after 8 hr of heating.

After operations, an attempt to melt the seals was made with the upper heater Variac settings reduced to 50% and the lower heater-control temperature setting remaining at 380°F. The small plug rotated after 9 hr of heating. The large plug did not rotate until after the upper

heater Variac setting was increased to 60%. A total of 48 hr heatup time was required for the large plug.

Both plugs were vacuum cleaned; 0.38 lb of oxide was removed from the small plug, and 1.22 lb of oxide and metal were removed from the large plug. In addition, 3.82 lb of metal was removed from both plugs. Temperature measurements by means of a thermocouple probe have been taken which indicate a maximum liquid alloy temperature of approximately 380°F on the trough bottom and a minimum surface temperature of approximately 250°F.

An inter-Divisional Laboratory committee appointed to investigate the problem of the seals held its first meeting on October 8. Its recommendations for the present are to continue to "vacuum clean" the seals and to continue operating the seals with reduced heat input to limit alloy oxidation.

c. Control Rod Drives. Control rod drive No. 9 (see Progress Report for September 1965, ANL-7105, pp. 1-2), which had previously been removed from the reactor, was disassembled because of the inability to free it up by normal washing operations. Sodium had migrated above the upper bellows due to failure of this bellows. Sticking of the sensing rod was due to the presence of frozen sodium between it and the gripper tube. The lower bellows was also found to be deformed. New bellows, on order, are expected to be received by the end of the month. New end pieces have been fabricated and tubing ordered to replace the parts damaged in disassembly.

Because of the difficulty experienced with the present rod drive in control rod position No. 9, special provisions were made for operation this month. The stainless steel rod from position No. 8, which had been used for reactor kinetics measurements, was moved to position No. 9 by exchange with the control rod in that position. The stainless steel rod was maintained in the "down" position by lowering the drive shaft so as to be in contact with it. The gripper jaws were left in the open position, and the drive was made inoperative. Since the required number of operating control and safety rods were available, no conflict with safety requirements was involved.

d. Bulk Sodium--Reactor Cold Leg Temperatures. In order to determine the coolant temperature rise across the reactor, the temperature of the inlet sodium is measured at the pump inlets by means of resistance thermometers. During recent operation, the resistance thermometer at the inlet to primary sodium pump M1 failed (because of low resistance to ground) and was replaced by summing the two thermocouples at approximately the same location. To maintain a balanced system, the resistance thermometer on the M2 side was replaced by the three thermocouples in

approximately the same location. The five thermocouples are connected to form the cold leg for the reactor ΔT circuit.

e. Fuel Element Rupture Detector Instrumentation. In an effort to quiet spurious noise in the neutron-counting instrumentation, the low-level inputs were all raised above ground, the power input regulated with an electronic regulator and filtered, and the low-level amplifiers relocated closer to the detectors. Each conductor carrying a low-level signal between detectors and pulse amplifier was treated as a source of noise pickup and placed in a separate length of copper tubing. This modification was partially successful, but some noise is still evident when certain components of the fuel-unloading equipment are started. Additional effort to reduce the noise bursts will be made on the signal lines between the depressed area in the Reactor Building and the junction box to the Control Room.

During the rework period, checks were made of the counting capabilities of the detectors. The BF_3 detectors are most sensitive, and the background noise is down by a decade over that of the boron-coated counters. The attenuation was varied and the best fit determined.

f. NaK-filled Pressure Transducer Test. The new differential pressure cell on test in parallel with the existing one in the Foster flow-meter of the secondary sodium system continues to provide information and has been considerably more stable than the present units operating under similar conditions. During an attempt to simulate primary tank conditions by heating part of the capillary tubing, the heating tapes failed prior to test completion. The tubing will be rewrapped and the test continued.

g. Interbuilding-coffin Power Supply and Monitoring Instrumentation. A power supply has been added to the interbuilding coffin to serve as its normal source when the coffin is not in transit. The existing battery source on the coffin has been retained and will serve as the emergency supply. The new power supply is a diode-bridge operating from a step-down voltage transformer connected to the 120-V a.c. building system. Indication for temperature and flow, as well as for alarm and cooling pump discharge pressure, have been added for monitoring of the element loaded in the coffin.

3. Reactor Improvements

a. Oscillator System, Mark II. A new oscillator rod system, Mark II, is being designed to facilitate the monitoring of reactor kinetics in EBR-II and allow much greater flexibility in the acquisition of necessary data. The fabrication of several components is underway.

The oscillator is a rotary device to be installed in a control drive and rod location. It is fully compatible with the fuel-handling system, and will not cause any delay during the starting and finishing of fuel-oscillator rod will be loaded or unloaded via the

fuel-handling gripper mechanism, transfer-arm mechanism, and fuel-unloading machine, and thus will not require any special tools or shielding coffins.

The oscillator rod (see Fig. 1) consists of an outer tube that contains four eccentrically located cylindrical inner tubes, two of which are loaded with approximately 75 g of B_4C . The centers of the cylindrical tubes are approximately 17 mm from the center of the outer tube, which can normally be rotated at speeds from 0.002 to 2.000 rotations/sec, and for a limited time, up to 10.000 rotations/sec. The tubes containing the B_4C are connected to a gas expansion chamber of approximately 800 cm³. This will permit 1 a/o burnup of all boron atoms before increasing the internal pressure by 4 atm, assuming 100% gas release.

The oscillator rod outer tube is topped by a quasistandard fuel-subassembly upper adapter; its bottom end connects to a bearing assembly that fits into a standard control rod thimble. The bearing surfaces are made of Colmonoy No. 4 and Stellite 6B. The bearing assembly is anchored to the reactor support grid during oscillator operations, but is completely removable.

The oscillator drive (see Fig. 2) connects to the oscillator upper adapter with a gripper that is similar to the control drive grippers. It has two flat areas on the gripper jaw teeth which bear against matching flats on the upper adapter and thus transmit the rotary motion. A 28-ft-long rotating shaft assembly extends upward through the shield plug and through a pressurized packing seal. Then it connects to the variable-speed motor drive and gear assembly as well as to the sensing and jaw-actuating devices. The rotating shafting is contained inside a guide tube extending from the top of the shield plug through the bulk sodium and through the reactor vessel cover into the upper plenum of the reactor vessel. The guide tube houses four bearings spaced about 7 ft apart. Two bearings are submerged in sodium and are made of the same materials as the above-mentioned oscillator rod bearings. The other two operate in the argon blanket, and are made of Colmonoy No. 5 and Aluminum Bronze, Ampco No. 22. All bearings are removable. The guide tube is suspended from a force-sensitive device that detects any significant friction during vertical travel of the reactor vessel cover.

The sensing, actuating, and driving devices are mounted on the control drive lifting platform and operate in air at room temperature. Appropriate control cables lead to the oscillator console in the control room.

Several component tests, as well as a performance test of the complete oscillator in sodium, are planned before its installation in EBR-II.

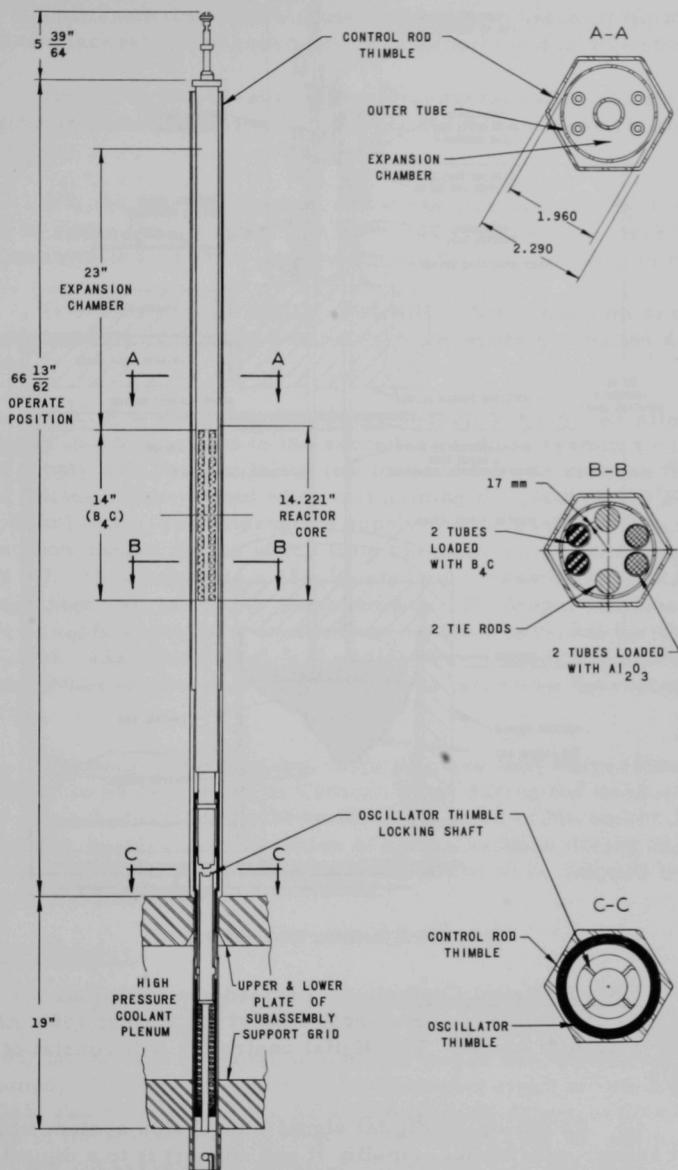


Fig. 1. EBR-II Oscillator Rod--Mark II

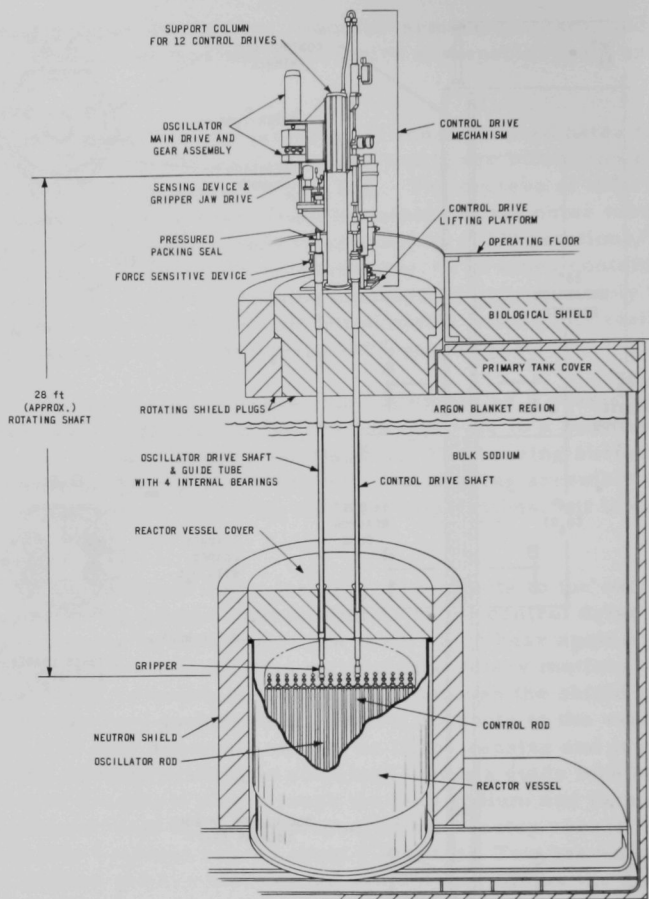


Fig. 2. EBR-II Oscillator Drive--Mark II

b. EBR-II Digital Controller. Revised specifications for the EBR-II digital controller (see Progress Report for August 1965, ANL-7090, pp. 3-5) have been prepared. The digital controller will consist of six main components:

- (i) An analog-to-digital signal-conversion system which will take plant sensor information, amplify it and convert it to a digital format capable of being used by the digital computer.
- (ii) A general-purpose digital computer which will perform all the arithmetic and logical control functions as well as coordinate controller activities.

(iii) Real-time and elapsed-time clocks which perform the timing functions necessary for coordination of programs and activities.

(iv) A digital-to-analog signal-conversion system which converts digital information to analog voltages for use in displays and simulation.

(v) An "on-off" control and sense line system which allows the computer to sense the presence of a specified voltage (will check the condition of an interlock or relay) and which allows the computer to close relays.

(vi) An operator-digital controller communication system which allows the exchange of information between the operator and the digital controller.

c. A.C. Em Pump for Secondary Sodium System. An alternative power supply has been added to the secondary sodium system a.c. em pump. This new supply will be used in the low forward flow or reverse flow (to counteract natural convection) when maintaining the plant at 700°F standby with electrical heat. The alternative supply will be switched into service in the low-flow range, during which time the main motor generator set will be turned off. This supply is a 480-V-input auto transformer which feeds low-voltage high current to the pump winding. By proper interlocking, the alternative supply operates from common controls provided for the motor generator set. Experience during the last standby condition showed this auto-transformer control to be much more reliable than the motor generator set control.

d. Primary Tank Heaters. Two primary tank immersion heaters are scheduled to be completed in Central Shops during the week of November 8 and are scheduled to arrive in Idaho the week of November 15. The remaining four heaters are scheduled to arrive in Idaho during the month of December. The heater elements are scheduled to be shipped from the factory by the end of October.

4. Reactor Physics

a. Radial U^{235} Flux Distribution. The fission rate distributions were calculated for EBR-II by multigroup, two-dimensional analysis.¹ Two sets of confirming experimental data on the radial flux distribution have been obtained: one from flux-wire measurements made at low power in March 1965, and a second by the EBR-II Analytical Group in determining the burnup in the maximum, minimum, and central fuel-pin positions of several of the subassemblies removed during the fuel-surveillance program.

¹See Koch, L. J., Lowenstein, W. B., and Monson, H. O., Addendum to Hazard Summary Report for Experimental Breeder Reactor-II (EBR-II), ANL-5719 (Addendum) (June 1962).

Relative data were obtained by normalizing the burnup data to the pin with maximum burnup in the Row 2 subassembly. A minor correction must be made to this burnup data to account for the U^{238} contribution to the burnup. These are all given in Fig. 3. The agreement is quite satisfactory. Flux-wire measurements are planned for the future, and measurements of irradiated fuel pins will be made on a continuing basis.

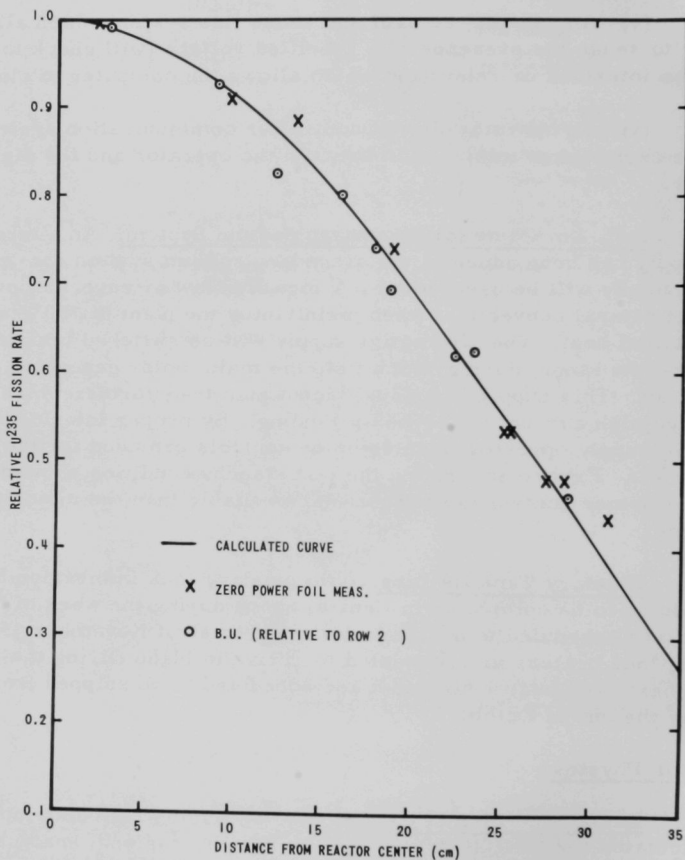


Fig. 3. U^{235} Radial Fission Rate Distribution in EBR-II

b. Reactivity Monitoring. Data from rod-drop measurements have been analyzed and show no significant change in the prompt feedback reactivity coefficient between the initial data obtained at 1630 and 2003 MWd taken in May 1965 and 3320 MWd taken in September 1965. Table I shows the results of the recovery of reactivity within 0.5 and 1.0 sec after initiation of the drop of the stainless steel rod. This is equivalent to 17 Ih ($4.1 \times 10^{-4} \Delta k/k$) reactivity worth.

TABLE I. Recovery of Reactivity

MWd	Recovery, $\Delta k/k$ ($\times 10^4$)	
	0.5 sec	1.0 sec
1630	0.50	0.70
2003	0.38	0.62
3320	0.42	0.68

5. Fuel Surveillance

A tentative burnup limit of 1.2% has been set on the basis of sodium-bond height and volume measurements obtained with several fuel elements removed from subassembly C-104. These measurements indicated that the maximum increase in fuel volume is

near 7.8%. At this point, small increments of increase in fuel volume result in large increases in internal jacket pressure.

Two additional fuel rods with burnup of 1.0 a/o have been furnace heated (see Progress Report for September 1965, ANL-7105, p. 4). After the 750°C treatment these two rods displayed evidence of volume increases, but not to the extent previously observed at 1.0 a/o burnup. Both rods failed by eutectic melting during a final treatment at 800°C. The results are shown in Table II.

TABLE II. Results from Furnace Heating Tests of EBR-II Jacketed Fuel Rods

Rod No.	Temperature, °C	Average Diameter, mm	Volume Change, %
E-25	Start	4.547	-
	600	4.445	+0.06
	650	4.420	+0.06
	700	4.420	+0.03
	750	4.445	+0.20
	800	Ruptured	-
E-33	Start	4.496	-
	600	4.445	+0.20
	650	4.445	+0.21
	700	4.420	+0.16
	750	4.420	+0.30
	800	Ruptured	-

Upper blanket rods have been received from subassemblies C-140 and C-143 which were removed from EBR-II following exposures to 0.26 and 0.50 maximum a/o fuel burnup, respectively. The blanket rods have been examined for evidence of growth of the depleted uranium at these relatively low-exposure levels. Dimensions (length and diameter) were within the design values for both levels of burnup, although diameters of bare slugs with the higher exposure were slightly larger. Density measurements

on one-inch sections of the 0.26 a/o material from the top of the top slug to the bottom of the bottom slug did not reveal a significant trend. Density measurements on the 0.50 a/o material have not been completed.

Further examinations and tests with irradiated fuel may provide evidence that the allowable burnup in the Mark-I fuel can be raised to some higher level. However, pending further investigations, the reactor loading is being programmed so as not to exceed the 1.2% maximum allowable burnup in any subassembly.

In addition to the subassemblies having 1.2% burnup, one subassembly from Row 4 with approximately 1.07% burnup and one control rod with approximately 1.0% burnup were removed for additional surveillance measurements.

6. Fuel Cycle Facility

About 931 elements were decanned during this period. It was necessary to replace a drive sprocket on the decanner scrap cutter as a result of excessive wear of the sprocket teeth.

Twelve melt-refining runs, and the corresponding skull-oxidation runs, were completed. The ingot yields ranged from 91.6 to 96.6%.

An induction feedthrough failed due to what appears to be a breakdown of the insulation as a result of moisture on the magnesia insulation. This feedthrough has been repaired and reinstalled.

The induction coil on melt refining furnace B failed due to melting of a $1\frac{1}{2}$ -in. section of the copper coil. This appears to be a result of a crack in the furnace insulation which allowed the susceptor, which operates at about 1600°C, to radiate heat to the coil. A replacement unit is being fabricated.

Twelve injection casting runs were made in which the average yield of metal cast was about 80 g, or almost the theoretical amount. However, in the processing of 1,123 molds from eleven injection casting runs, the yield of acceptable castings was only 42%. The cause of this decrease in acceptable yield (normally about 65%) is not clear. Investigation of this problem by variation of the casting parameters is under way. Assembly, welding, leak-testing, bonding, and bond testing produced 817 acceptable elements. Eight core-type subassemblies were fabricated.

The blanket decanner (see Progress Report for September 1965, ANL-7105, pp. 8-9) has been received at Idaho. The unit provides for wheel-cutting of the blanket cladding and pressing of the uranium out of the cladding by a pneumatic cylinder. It is operated in conjunction with the

fuel-element decanner and utilizes the same control and feedthrough system. The decanner has been set up in the mockup area for testing and training purposes, and will be used initially in sampling both axial and radial blanket material to determine alloy stability under irradiation, and to obtain breeding data. It will be available later for decanning blanket material for processing.

B. FARET

1. General

There has been practically no change in the status of the Architect-Engineer's portion of the Title II design during the month. The design is essentially complete and all design packages have been signed and issued, except Packages V and IX. These design package drawings and specifications have been ready for signature since early June 1965. Approval is being withheld until firm guidance has been received from the Commission relative to the start of construction.

The Laboratory is continuing to review drafts of UE & C-prepared bid invitations for various FARET equipment. Recent material submitted for review have covered inspection and testing services, roof decking, siding, and miscellaneous piping.

The current delay in authorizing the initiation of Title III continues to multiply schedule and cost-estimating problems.

2. Reactor Vessel

The preliminary design phase of the reactor vessel and internals includes defining of the design details of both components and the preparation of reference drawings, shop procedures, stress analyses, and cost and time estimates for shop fabrication. The reactor vessel vendor, the Babcock and Wilcox Company, is expected to complete the preliminary design report early in November. This report was originally scheduled for September, but difficulties in designing a clamping arrangement for the vessel cover and an extension piece to the reactor cover seal have caused a delay.

The preliminary design study has confirmed much of the original vessel concept and has also indicated two areas which will probably require some experimental verification prior to final fabrication. The first concerns the flow dynamics of the sodium coolant in the main-inlet, high-pressure plenum and in the mixing-chamber box, located in the coolant outlet region of the core subassemblies. The second is that of determining an appropriate gasket design and seating pressure to use for the cover-to-extension-piece seal joint. This joint design is made difficult by the conflicting requirements of low leakage and easy removal of the reactor vessel

cover for fuel handling and experimental work with instrumented subassemblies. The basic problem is concerned with leakage rates. A high seating pressure will insure a tight joint but requires cumbersome cover-locking mechanisms. A proof test is being considered to determine the best combination of gasket design and seating pressure.

The availability of the special 304 stainless steel for the reactor vessel has been questioned. Two vendors have indicated acceptance of the stringent specifications, with the exception that the ASTM grain size will be quoted as somewhat coarser than specified. The vendor response to the vessel plate material was also encouraging; the only material exceptions were that the silicon may be 0.75% maximum instead of specified 0.50% maximum, and the nickel may range from 11 to 12% instead of the specified 11.5 to 12%. Vendor quotations do indicate, however, that the silicon and nickel constituents be as close to the ANL specifications as possible. These slight deviations will be reviewed in detail, although none of them appear to be serious, and the original intent to maximize ductility appears both reasonable and attainable.

A joint review of the preliminary vessel design by ANL and B&W indicated considerable conservatism in the design while maintaining a high degree of experimental flexibility for the FARET program. B&W calculations have shown that many areas of the vessel need not be protected by thermal baffles or shields. However, the baffles have been incorporated as additional protection.

3. Seismic Analysis of Piping for Sodium

The Laboratory has engaged John A. Blume and Associates, Engineers, San Francisco, to investigate the dynamic seismic stresses and displacements of sodium piping critical to safety. The work includes determination of earthquake exposure of the FARET site, a design-criteria report, and dynamic analysis of piping. The work is expected to be completed in November 1965.

However, the need for additional work has been indicated as a result of meetings with members of the ACRS and the AEC Division of Reactor Licensing. A listing of structural equipment critical to safety has been compiled which will be submitted, along with the FARET seismic design philosophy, to J. A. Blume and Associates for their review. In particular, the review is intended to evaluate the adequacy of the design approaches and whether dynamic analyses may be required for certain items of structure or equipment.

4. Cell Operating Handling Mockup

Figure 4 illustrates, in part, a FARET cell operations handling mockup to be used primarily in the preliminary investigation of in-cell handling problems associated with (a) material handling, (b) equipment operation and replacement, and (c) removal and replacement of cell-wall electrical and pneumatic penetrations. Complete fuel-handling operations are not contemplated.

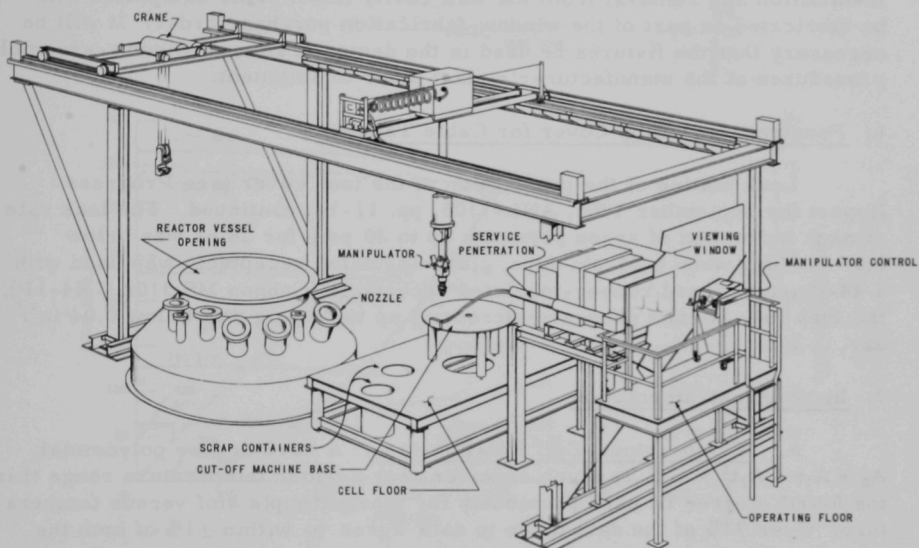


Fig. 4. FARET Cell Handling-operations Mockup

Relative component elevations of the mockup reproduce those anticipated for the FARET cell. The craneway, operating floor penetration, and window are stationary. Provisions have been incorporated to allow repositioning of equipment relative to the window structure. As shown in the figure, the floor structure is raised to permit inclusion of subfloor storage holes and the subassembly cutoff machine equipment pit. By means of the mocked-up window, the top section nozzles of the reactor vessel can be observed for replacement of instrument leads.

Handling operations will be performed with the crane and/or manipulator to establish limits of operational procedures.

The craneway, the window with its support, and the cell floor structure have been installed. The penetration unit, crane, operating floor, and top section of the reactor vessel are available for immediate installation.

A surplus manipulator together with mockup lighting will be utilized as soon as these are available within the next few months.

5. Shielding Windows

Additional drawings have been made of special fixtures needed for handling the "A," "B-1," and tank subassemblies (see Progress Report for September 1965, ANL-7105, p. 12, Fig. 5) of the shielding window during installation and removal from the wall cavity liner. This equipment will be fabricated as part of the window-fabrication purchase order. It will be necessary that the fixtures be used in the demonstration of window-assembly procedures at the manufacturer's plant prior to shipment.

6. Penetration of Tank Cover for Cable Take-up

Leak testing of the penetration of the tank cover (see Progress Report for September 1965, ANL-7105, pp. 11-14) continued. The leak rate at each increment of argon pressure up to 30 psig for 24 hr was below 0.06 in.³/day when a 24-pin-type, glass-insulated receptacle was used with a 44-pin-type, hard rubber-insulated receptacle (Cannon MS 3102 C 44-1P), the leak rate at each pressure increment up to 30 psig was below 0.04 in.³/day.

7. In-core Instrumentation

a. Temperature-Emf Relationships. A third degree polynomial, $A_0 + A_1t + A_2t^2 + A_3t^3$, is much superior over a wider temperature range than the fourth-degree fit used previously for thermocouple emf versus temperature. Over 97% of the data taken to date agree to within $\pm 1\%$ of both the manufacturer's average value as well as the least-square values. Because of the very minor changes in the measured table values and because the current average values generally agree with those found by others,² no further work will be devoted specifically to further correlation.

b. The Resistivity of Refractory Oxide Insulators. (Correction to Progress Report for September 1965, ANL-7105, p. 16.) It was stated that one of the reasons for selecting thoria as an electrical insulation was "(iii) It has low electrical resistivity at temperatures above 2300°C." This is definitely incorrect and should be replaced by the statement "... that the actual value of resistivity of thoria at temperatures above 2300°C has been reported low." This is a definite disadvantage of considering this material. The lower the material resistivity, the greater will be the thermocouple errors caused by insulation shunting effects.

²GEAP-4864, Quarterly Progress Report, SEFOR Project (May 1965).

8. Fuel Assembly Sodium Flow Test Loop

The new 800-gpm sodium pump has replaced the interim pump. The test performance data obtained at the vendor's plant are shown in Fig. 5 together with the system hydraulic requirements.

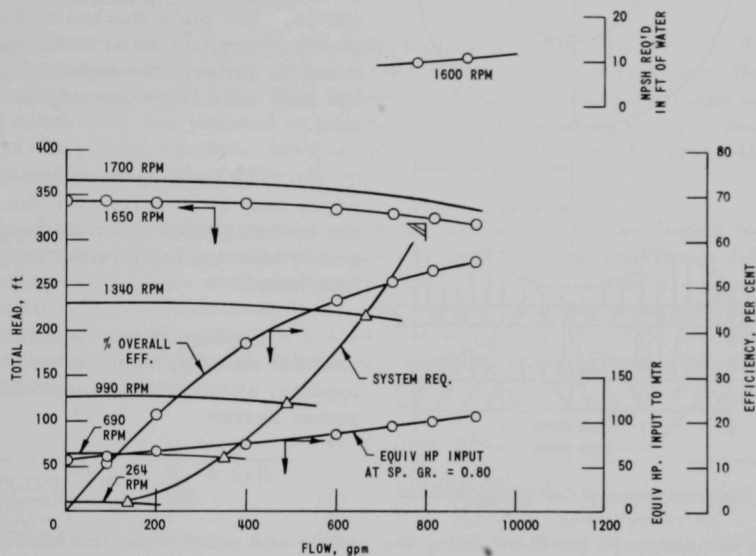


Fig. 5. Pump Test Performance

The Conax fitting which connects the pump discharge line to the downcomer into the high-pressure plenum of the test fuel-assembly inlets is being welded to the reducer at the pressure-vessel inlet. The existing 4 x 10-in. reducer will then be cut out of the pressure vessel and this new Conax-reducer assembly welded into the pressure vessel. The 2-in. dump lines are completely insulated, and the 3-in. overflow line is about 90% completed.

9. Stress Analysis of Core Support

A computer analysis of the core support has been finished. The structure analyzed and the convenient solution provided by the computer program can best be made clear by the cross-sectional view of the structure shown in Fig. 6.

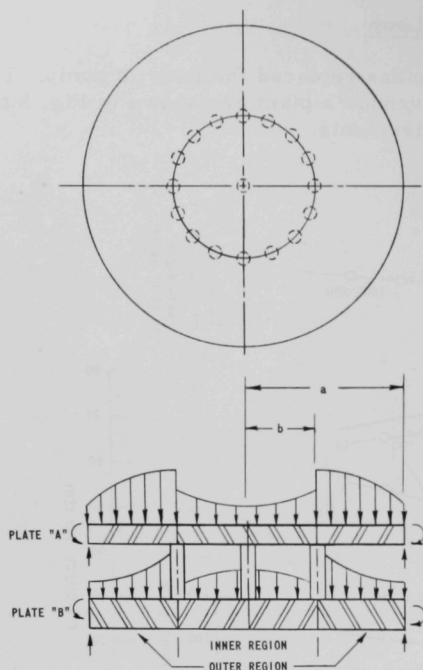


Fig. 6. Diametral Section of Core Support Structure

and a temperature gradient along the radius and across the thickness, which is expressed by a double power series

$$T(r, z) = \frac{z}{h} \sum_{m=1}^{\infty} A_m r^m + \sum_{n=1}^{\infty} B_n r^n,$$

where

$f(r)$ - intensity of transverse pressure, lb/in.²

$T(r, z)$ - steady temperature distribution, °F

h - plate thickness, in.

r - radius of plate, in.

A, B - constants dependent on temperature distribution

F_m - constant dependent on pressure distribution

The statically indeterminate structure consists of top and bottom axisymmetric plates connected by an axial load member in the center, and a concentric ring of tubes located at a radius b . The plates are made up of two regions where the planar areas of the regions are the same for both plates. The plate thicknesses or physical properties of each region must be uniform throughout any region but may vary from one region to the next.

The bending restraint at the edges may be different for the top and the bottom plates and may range anywhere between completely free to fully fixed.

Loading of the structure is twofold, namely, transverse pressure loading, which is represented by the power series

$$f(r) = \sum_{m=1}^{\infty} F_m r^m,$$

The loading of transverse pressure or temperature gradients may be different for all the four regions. They are continuous, however, in any respective region.

The computer program gave the plate deflection, radial and tangential stresses due to transverse pressure, and temperature gradients at specified intervals. The membrane stresses in the plates caused by the temperature variation along the radius were also found. These membrane stresses are for the particular case of plates not restrained from axial motion at the edges. Stresses and maximum displacement of the tubes were also given.

10. Reference Core-I Design

The primary objective of experiments with the first core in FARET is the test and verification of fast-reactor fuel elements typical of the type to be used in a fairly large fast power reactor. The Core-I-design operating conditions are planned to bracket the corresponding design specification of the power reactor. Several different fuel-element designs will be tested under instrumented conditions.

The Core-I design will consist of carbide, metal, and oxide fuels in subassemblies driving each other and will test simultaneously ten different fuel-element designs with good statistics.³ The Core-I data are given in Table III. The fuel-element types, and designs, and the tentative conditions of operation are presented in Tables IV and V. The elements are typed according to fuel material, fabrication method, cladding material, and/or thermal conditions.

TABLE III. Core I Data

<u>Entire core</u>		<u>Radial reflector</u>	
Equivalent diameter, in.	17.5	Height, in.	80
Height, in.	18	Equivalent outside diameter, in.	42.3
Volume, liters	70	Radial thickness, in.	13.1
<u>Subassemblies</u>		<u>Radial reflector composition, v/o</u>	
Mixed oxide	24	Stainless steel	82
Mixed carbide	16	Sodium	18
Pu-U alloy	8	<u>Heat output, MW</u>	
Special subassemblies	3	<u>Primary sodium temperature, °F</u>	
Control rods	12	To core	810
Radial reflector (including loops)	238	From core (nominal)	1050
Total	301	<u>Primary sodium flow rate</u>	
Configuration	Hexagonal	Through core, gpm	6000
Dimension across flats, in.	2.290	Core pressure drop, psi	80
Lattice spacing, in.	2.320		
Tube-wall thickness, in.	0.040		
<u>Control-rod composition, v/o</u>			
Boron carbide	55		
Stainless steel	20		
Sodium	25		

³Persiani, P. J., Bump, T. R., and Kann, W. J., FARET Core I Fuel Irradiation Program and Reference Design, ANL-7106 (October 1965).

TABLE IV. Fuel-element Data

Fuel Material	UO ₂ -15 w/o PuO ₂	UC-15 w/o PuC	Metal ^b
Elements per subassembly	37	37	61
Fuel height, in.	18	18	18
Clad outside diam, in.	0.290	0.290	0.220
Clad thickness, in.	0.020	0.020 ^a	0.016
Spacer wire diam, in.	0.057	0.057	0.052
Axial blanket height (each end), in.	6	6	6
Gas reservoir, in.	25	25	25
Element height, in.	55	55	55
Effective fuel density, %	80	80	70
Bond material	Helium	Helium	Sodium
Fuel U/Pu atom ratio	6/1	6/1	5/1
Fuel details	Coprecipitated; O/M 1.97-2.00	Single Phase; Solid Solution	-

^a0.015-in. C4 subassemblies.^bU-15 w/o Pu-6.5 w/o Ti; U-15 w/o Pu-10 w/o Zr (see Table V).

TABLE V. Subassembly Data

Fuel Material	Subassembly Designation	Fuel Type	Clad Material	No. of Subassemblies	No. of Instrumented Subassemblies	Maximum Linear Heat Flux (Design), kW/ft	Maximum Clad Temp, °F (°C)	Maximum Fuel Temp, °F (°C)	Burnups ^a at Removal, a/o	Maximum Clad Thermal Stress, psi	Coolant Velocity, ft/sec
Oxide	O1	Pellets	304	4	1	15 1250 (675)	3220 (1770)	5, 9, 12, 14	13,300	16	
	O2	Pellets	304	4	1	22 1290 (700)	4220 (2330)	5, 8, 10, 12	19,400	23	
	O3	Vipak	304	4	1	15 1250 (675)	3220 (1770)	5, 9, 12, 14	13,300	16	
	O4	Vipak	304	4	1	22 1290 (700)	4220 (2330)	5, 8, 10, 12	19,400	23	
	O5	Pellets	HSA	4	1	22 1340 (725)	4250 (2340)	5, 9, 12, 15	-	20	
	O6	Vipak	HSA	4	1	22 1340 (725)	4250 (2340)	5, 9, 12, 15	-	20	
Carbide	C1	Pellets	304	4	1	15 1250 (675)	2030 (1110)	5, 9, 12, 14	13,300	16	
	C2	Vipak	304	4	1	22 1290 (700)	2520 (1380)	5, 9, 12, 14	19,400	23	
	C3	Pellets	HSA	4	1	29 1340 (725)	3050 (1680)	5, 9, 12, 15	-	30	
	C4	Vipak	HSA	4	1	36 1340 (725)	3390 (1870)	5, 9, 12, 15	-	39	
Metal	M1	U-Pu-Zr	HSA	4	1	14 1250 (675)	1580 (860)	5, 9, 12, 14	-	20	
	M2	U-Pu-Ti	V-Ti	4	1	14 1250 (675)	1580 (860)	5, 9, 12, 14	-	20	
Advanced	C4S	-	-	3	3						
				51	15						

NOTES: 1. Vipak means "vibratory compacted"; HSA means "high-strength alloy," not necessarily the same for oxide as for carbide, etc.

2. Coolant inlet temperature is 810°F. Average outlet temperature from each subassembly is 1050°F. (Exception: outlet temperature from O5 and O6 subassemblies is 1085.) Axial peaking factor = 1.2.

3. Maximum clad temperature include both a 1.33 factor for flow and power maldistribution effects on coolant temperature rise, and a 1.10 uncertainty factor. Maximum fuel temperatures include the 1.33 factor but no uncertainty factor.

^aApproximate burnup intervals.

The assumptions used in the thermal calculations, basic to the core design and thermal analysis, are shown in Table VI.

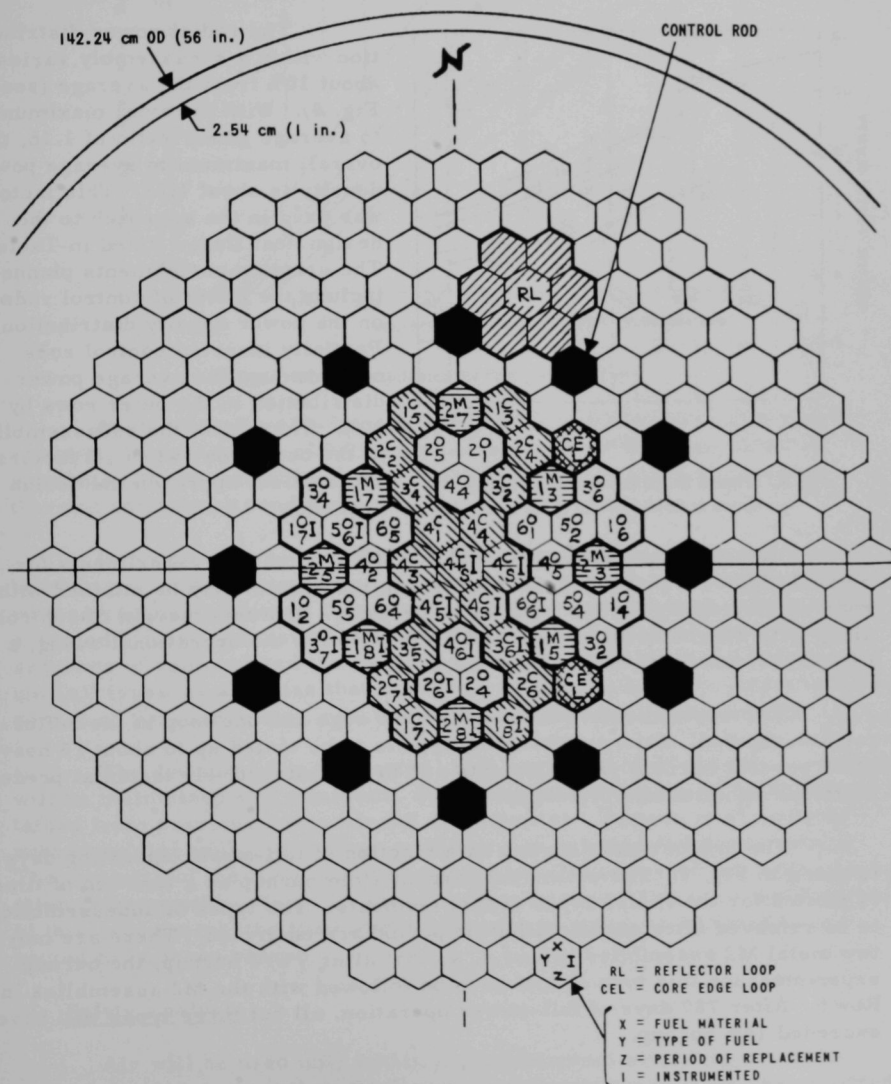
TABLE VI. Assumptions for Thermal Calculations
(Based on a sodium film coefficient of 20,000 B hr⁻¹ ft⁻² °F⁻¹)

Fuel Material	Clad Thermal Conductivity, B hr ⁻¹ ft ⁻¹ °F ⁻¹	Fuel-clad Interface Conductance, B hr ⁻¹ ft ⁻² °F ⁻¹	Fuel Thermal Conductivity, B hr ⁻¹ ft ⁻¹ °F ⁻¹
Oxide	13.5	1,500	1.7 ^a
Carbide	13.5	1,500	10
Metal	14.5	40,000 ^b	9 ^b

^aThe fuel is assumed to have a central hole large enough to produce an "effective" fuel density of 85%, provided that the remainder of the jacket interior is filled with fuel of 100% density. This condition reduces the temperature rise through the fuel to 67% of that through a solid fuel pellet. The central hole is expected to form in oxide at centerline temperatures above 1600-1800°C.

^bThe fuel is considered to have expanded against the jacket, displacing the bond sodium, and to have an accompanying reduction in thermal conductivity.

The core configuration is shown in Fig. 7. Several conditions were considered in the positioning of the subassemblies. Symmetry was maintained as closely as possible to simplify analysis and to subject the several elements of each type to similar power conditions throughout the experiment. Also, to achieve the linear heat fluxes, the uranium enrichment and positions in the configuration were varied.



Configuration for FARET Core-I Experiment

The positioning was also influenced by the sequence of removal and replacement. Instrumented subassemblies are usually located so that the loading and unloading of other subassemblies is not made cumbersome by having instrumentation leads located over subassemblies to be removed. It is planned to remove the instrumented subassemblies in the latter stages of burnup for each type element.

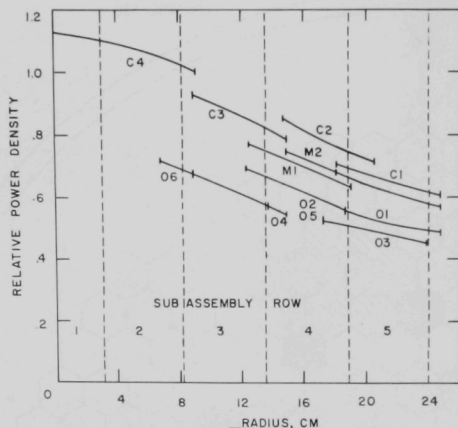


Fig. 8. Relative Radial Power Density Distribution at Core-I Center Plane

The radial power distribution within a subassembly varies about 10% from the average (see Fig. 8). With the axial maximum to average power ratio of 1.16, the overall maximum to average power density is about 1.28. This factor was used in the approach to the design heat fluxes listed in Table V. The uranium enrichments planned include the effect of control rods on the power density distribution. Partially inserted control rods could reduce the average power distribution in the outer rows by 10%. Therefore, the subassemblies in the outer row, when all factors are applied, approach the design heat flux.

Computations, along with related ZPR-3 critical experiments for FARET, indicate that a 10% reactivity-control system may be attained with rods employing highly enriched boron carbide. With this margin of control along with 2% shutdown margin and 2% margin for the operational swing, a 6% excess reactivity can be used for burnup.

Two experimental loops at the core edge and one loop in the reflector are planned. Each subassembly type is to be tested up to about 15 heavy atom percent burnup. The elements are to be destructively tested at predetermined subintervals of burnup.

The present atom burnup as a function of full-power operating days is given in Fig. 9. The estimated percent atom burnup as a function of time is plotted for the twelve types of fuel elements. The types of subassemblies to be removed after each irradiation period are encircled. There are only two metal M2 assemblies in Row 4, so that after 9 a/o burnup, the burnup experiment for this type of fuel is to be followed with the M2 assemblies in Row 5. After 780 days of full-power operation, all but three types will have exceeded 14% burnup.

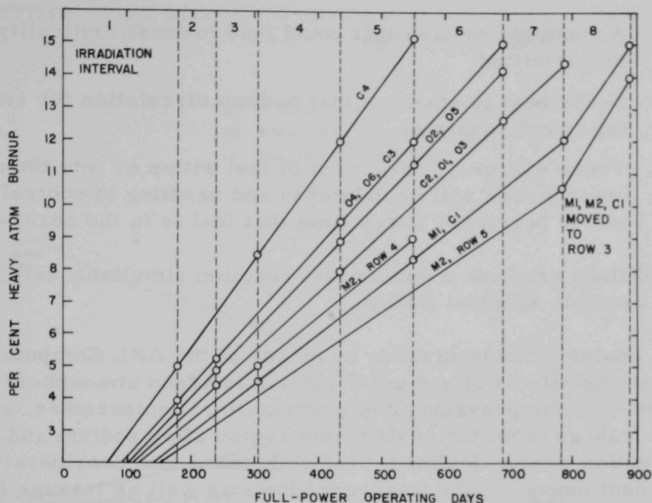


Fig. 9. Burnup Anticipated for Fuel-element Types

At the end of a 430-day operating period at full power (1.5 years, assuming a plant factor of 0.75), the performance of close to 1000 fuel elements (22 subassemblies) would have been investigated at advanced thermal and burnup conditions.

In order to go to burnups of 15 a/o, the necessary reactivity could be obtained by the replacement of some partly burned-up subassemblies with new subassemblies of the same design or of a new design. Alternatively, a few additional subassemblies could be added at the core edge. The sequence of removal and the replacing of subassemblies could continue until all types, or all those that have performed satisfactorily throughout the course of the experiment, reach a burnup of 15 heavy atom percent.

The downtime due to removal and replacement of the subassemblies will be maintained at a minimum, depending on the degree of confidence obtained from previous research and development. Inspection of removed subassemblies will give further confidence of satisfactory performance. The estimate of the time required for the usual loading and unloading operation is two weeks. Using an average plant factor of 75% over the duration of this experiment, the time to complete the program as outlined is expected to be three years.

11. Safety Analysis

Air will be used only within the containment structure when the reactor is shut down (subcritical) and the following conditions are satisfied:

1. A condition or task that could lead towards criticality will not be permitted.
2. Decay heat is small so that sodium circulation for reactor cooling is not required.
3. There will be no movement of fuel within or into the core. The control rods will be delatched and handling of control rods will not be permitted at any time that fuel is in the core.

These conditions preclude a sodium-air reaction simultaneously with a maximum credible accident (MCA).

An analysis has been made by means of the ANL Computer Code RE 327-X of the effects of sodium expulsion in argon atmosphere. Containment-volume pressure, containment-liner temperature, and total integrated leakage from the containment region after sodium and fission product ejection were calculated. The code takes into consideration the decay of the heat energy of the fission products as well as leakage from the containment region.

In the analysis, a transient heat balance is performed on the gas, inner and outer liners, concrete and steel webs of the containment structure. The webs, located in the cell structure, and the concrete are assumed to transport heat with equal temperature gradients, utilizing a composite conductance for the webs and concrete. The heat capacities of steel and concrete are also combined. For conservatism, a shrinkage gap between concrete and inner liner is assumed. Heat is ultimately dissipated through the containment structure to a constant temperature environment. Gas coolers are assumed to be inoperative during the transient. For the calculations, the walls were divided into three-inch nodes to allow for the poor thermal diffusivity of the concrete. This resulted in twenty-five simultaneous, first order differential equations which were solved using a subroutine employing a Runge-Kutta solution.

The results of the analysis are shown in Figs. 10 and 11, leakage being assumed proportional to the overpressure raised to the $1/2$ power. The results shown in Fig. 10 are for an assumed containment structure leakage rate of 30% of containment volume by weight per day at 30 psig (guaranteed leakage rate, not design leakage rate). The assumed leakage rate is considered an upper limit and yields pessimistic values of off-site doses following an MCA. The peak pressure of 3.5 psi occurs shortly after the expulsion. After 10^6 sec (about 11 days), the total integrated leakage is about 20% and the overpressure almost zero.

A zero-leakage case was calculated (see Fig. 11) to evaluate upper limits on pressure and temperature. The values for pressure and inner liner temperature peak at about 4×10^6 sec (46 days), being 4.3 psi and 277°F, respectively.

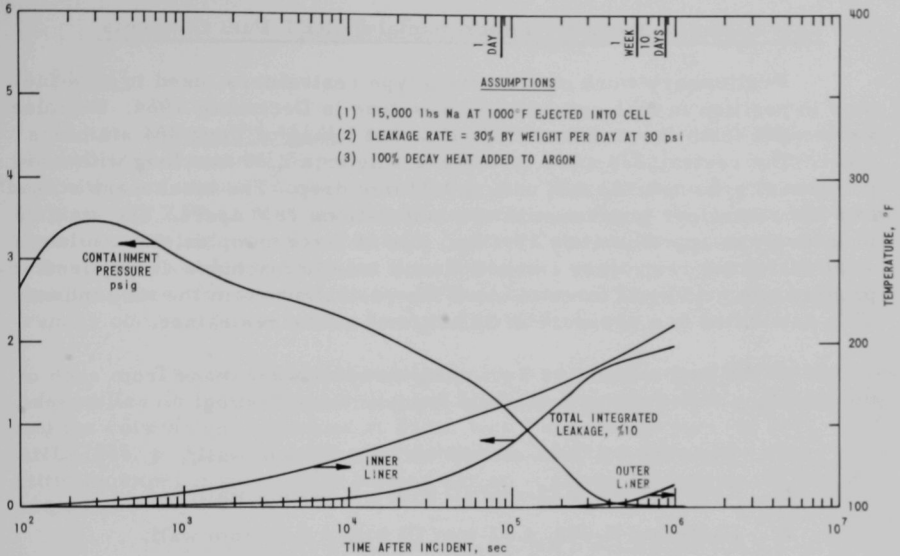


Fig. 10. Containment Pressure, Temperatures, and Leakage Following Maximum Credible Accident, with Containment-structure Leakage Rate of 30% of Containment Volume by Weight per day at 30%

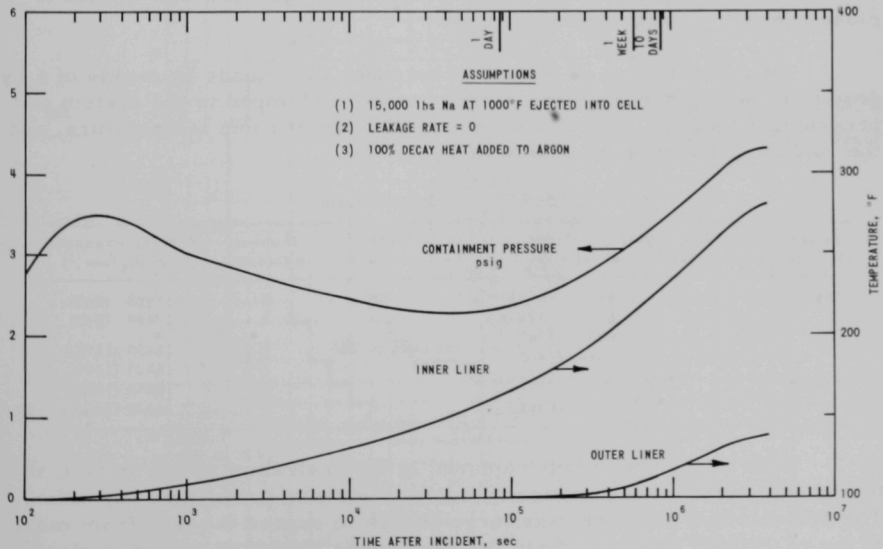


Fig. 11. Containment Pressure and Temperatures Following Maximum Credible Accident, for Zero Leakage Rate

12. Fabrication Methods for Experimental FARET Fuel Elements

Preliminary work on the crimp type restrainers, used to hold fuel pins in position in fuel-rod jackets, was done in December 1964. Samples were made from the standard EBR-II jacket tubing of Type 304 stainless steel. The restrainers were 3.94 mm diameter x 2.29 mm long with one peripheral groove 0.762 mm wide x 0.23 mm deep. The tubes were staked⁴ into the restrainer grooves with two indentations 180° apart. The staking pressure was approximately 18.2 kg. Ten of these samples, 2.5 cm long, were tested for restrainer extraction on a tensile machine. It required approximately 66.3 kg of force to move the restrainer from the tube indents. This calculated to a pressure of 563 kg/cm² on the restrainer.

In the past month five 3-in.-long samples were made from each of the following listed tubing materials for tube burst testing:

- a. Type 304 SS, 3.86-mm ID with a 0.23-mm wall;
- b. Type 316 SS, 4.22-mm ID with a 0.38-mm wall;
- c. Hastelloy X-280, 4.37-mm ID with a 0.38-mm wall.

Two specimens were staked with single-groove restrainers and two were staked with triple-groove restrainers. The fifth specimen was used as a control sample and did not have a restrainer. Plugs were TIG welded to close one end of each specimen.

Tube burst tests on staked jacket tubes were made by means of a hydraulic pressure system. The specimens were clamped to the system and pressurized with oil. The tests were performed at room temperature, and the rupture pressures are shown in Table VII.

TABLE VII. Tube Burst Tests

Jacket Material	Number of Grooves	Rupture Pressure, psi (kg/cm ²)	Jacket Material	Number of Grooves	Rupture Pressure, psi (kg/cm ²)
304 SS	1	8225 (580)	316 SS	3	11925 (840)
	1	8250 (582)		3	12000 (845)
	3	7900 (556)	Hastelloy X-280	1	16450 (1158)
	3	8275 (582)		1	16825 (1180)
316 SS	1	12075 (850)		3	16450 (1158)
	1	11875 (836)		3	16125 (1134)

None of the specimens ruptured in the restrainer area. In fact, the tubing diameter was less noticeably deformed in this area than any other. The deformation, however, was large enough to expand the tube from most of the restrainer grooves. Only two specimens remained staked in place. The control samples from each group will be tested in the near future.

⁴Staking is an operation in which one of two mating surfaces is deformed so as to key into a groove in the other. A special stakin

C. General Fast Reactor Physics

1. ZPR-3

a. Assembly 46LB. At the completion of experiments with Assembly 46G (see Progress Report for September 1965, ANL-7105, pp. 18-20) and with a minimum number of fuel changes. Experiment 46LB was performed with ZPR-3 to determine the relative worths of depleted uranium and stainless steel in a quadrant of both halves of the reactor blanket. Such information is needed to evaluate the effects of a proposed substitution of stainless steel for uranium in the EBR-II blanket. The Assembly 46 spectrum is comparable in hardness to that of EBR-II.

The axial blanket configuration was the same as for the previous Assemblies 46 (see Progress Report for February 1965, ANL-7017, p. 19), and the core height remained at 20 in. (see Progress Report for July, 1965, ANL-7046, p. 3). Figure 12 shows the core loading at the start of the substitution experiments. This loading had an available excess reactivity of 180.6 lh.

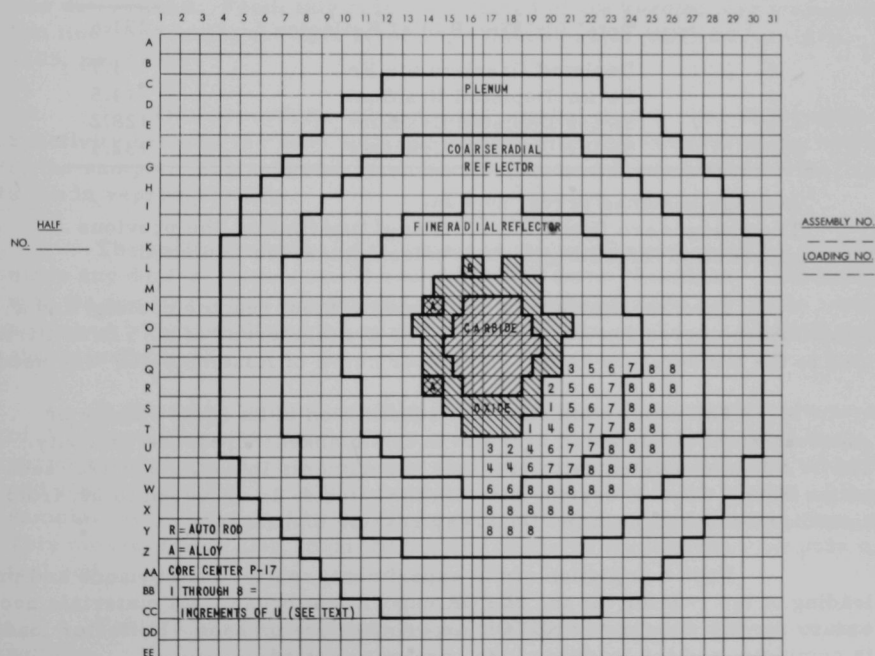


Fig. 12. Core-46LB Loading for Reflector-substitution Experiments

As indicated in the numbered positions of Fig. 12, 60.2 v/o depleted uranium was substituted, in increments, for stainless steel in the fine radial reflector; then 83.6 v/o depleted uranium was substituted for iron in a portion of the coarse radial reflector. Because of the low worth of this last step, the worth of iron for depleted uranium was measured in Position 1. Then the worth of stainless steel for depleted uranium was determined in the first two positions. The substitution height was the same as the core, 20 in. The worths for each increment are given in Table VIII.

TABLE VIII. Substitution Worths,^a Assembly 46LB

Position	Substitution	Worth, 1h ^b
1	Depleted Uranium for SS	-47.8
2	"	-38.7
3	"	-37.9
4	"	-44.5
5	"	-41.1
6	"	-43.0
7	"	-18.6
	Total for Fine Radial Reflector	-271.6
8	Depleted Uranium for Fe	-1.7
1	Fe for Depleted Uranium	+4.5
1	SS for Depleted Uranium	+28.2
2	SS for Depleted Uranium	+32.1

^a Average assumed error, ± 0.5 1h.

^b The changes are listed in the order of substitution, the previous substitution remaining in place unless otherwise indicated.

The experiment was performed without reactor cooling, and a temperature correction was applied. The average error of ± 0.5 1h is attributed to the temperature drift. The inhour curve of Assembly 46F was used.

The results indicate that substitution of an equal volume of stainless steel for depleted uranium in this blanket increased reactivity. The result is consistent with previous experiments in softer spectra, such as the Fermi Core-B design, and with the effects, as conveyed to us, from a similar substitution in the Dounreay reactor blanket.

Upon completion of the experiment, routine maintenance and pre-loading of the reactor for the SEFOR experiment began. All materials necessary for the start of the SEFOR experiment are on hand. Reflector loading is complete, and the loading of the core was started.

2. ZPR-6

The central worths of different samples were measured at the center of Assembly No. 4Z (see Progress Report for May 1965, ANL-7046, p. 14) by the following technique.

1. Criticality was achieved with the dual-purpose rods and with sample changer in the "in" position. The sample changer consisted of a drawer having the same composition as the central zone of the core with a voided front section ($2 \times 2 \times 1$ in.). Using an attached drive mechanism, the operator can insert or remove this drawer from the core remotely. The voided front section of this drawer was used for the sample whose worth is to be measured.
2. After criticality was achieved, the sample changer was removed (the power level started decreasing) and the equivalent of about 10 Ih was inserted through a special, nonscrammable control rod. When the desired low-power level was reached, the sample changer was inserted to its original position after a waiting period of not less than 5 min, the power level was determined. From this point, the period of the reactor was measured "on line" by feeding the data directly to the computer DDP-24 (see ANL-7105, pp. 57-8).
3. This procedure was repeated several times. The differences in reactivity between the runs with and without a sample measured the worth of the sample. The uncertainty in any measurement was based on the fluctuation in reproducibility.

The main advantage of this method is the elimination of the need to move any dual-purpose control rod which has some "backlash" associated with its position. The nonmovement of dual-purpose rods results in better accuracy. The results of the worth measurements of various materials are shown in Table IX.

It should be pointed out that in making certain worth measurements of B^{10} , Ta, and polyethylene, it was necessary to move a calibrated dual-purpose rod to counteract the large change in reactivity. Because of the odd shape of the Pu^{239} and U^{233} samples ($2 \times 2 \times 1/4$ in.), the worths of these samples were measured by inserting them manually in the sample changer. This measurement also required the use of the calibrated dual-purpose control rod.

Table X shows the worth of U^{235} as a function of thickness of the sample.

TABLE IX. Central Worths of Various Materials in Assembly 4Z of ZPR-6

Sample	Weight, g	Weight (and Composition) of Can, g	Gross Worth, lh	Net Worth, lh	Worth/kg, lh
Cd	499.50	26.97 (SS)	-4.598	-4.553 \pm 0.010	-9.115
W	1108.0	-	-5.742	-5.742 \pm 0.010	-5.182
Na	51.38	56.42 (SS)	-0.144 \pm 0.002	-0.049 \pm 0.005	-0.954
Be	114.308	-	+1.107	+1.107 \pm 0.010	+9.689
C	103.0	-	+0.194	+0.194 \pm 0.010	+1.883
SS (304)	499.60	-	-0.849	-0.849 \pm 0.010	-1.699
U ²³⁸	1153.80	-	-3.857	-3.857 \pm 0.010	-3.343
Li	28.30	57.03 (SS)	-0.691	-0.595 \pm 0.010	-21.024
SS Can	72.610	-	-0.122	-0.122 \pm 0.002	-1.680
Al	166.90	-	-0.297	-0.297 \pm 0.013	-1.779
B ₄ C	59.62	64.70 (SS)	-6.520	-6.410 \pm 0.025	-107.511
UO ₂	106.5	20.1 (Al)	-0.370	-0.334 \pm 0.015	-3.136
EuO	34.2	20.6 (Al)	-2.472	-2.436 \pm 0.025	-71.225
GdO	59.2	20.2 (Al)	-1.164	-1.128 \pm 0.025	-19.054
NaCl	58.175	26.1 (Al)	-0.150	-0.114 \pm 0.015	-1.959
DyO	104.70	20.1 (Al)	-2.062	-2.026 \pm 0.015	-19.350
Ni	546.0	-	-1.148	-1.148 \pm 0.010	-2.102
Fe	488.0	-	-0.739	-0.739 \pm 0.007	-1.510
Nb	481.2	30.10 (SS)	-3.842	-3.791 \pm 0.010	-7.878
Zr	406.0	-	-0.650	-0.650 \pm 0.005	-1.601
U ²³⁸	37.073	48.97 (SS)	-0.228	-0.141 \pm 0.022	-3.800
U ²³⁵	17.95 (total) 16.73 (25)	72.61 (SS)	+0.674	+0.803 \pm 0.022	+44.735
Polyethylene	59.15	-	+19.751	+19.751 \pm 0.010	+333.913
Mo	599.0	-	-3.415	-3.415 \pm 0.010	-5.701
U	183.67	55.30 (SS)	-0.231	-0.133 \pm 0.010	-0.72
Ta	924.70	27.54 (SS)	-11.956	-11.907 \pm 0.200	-12.87
B ¹⁰	33.30	55.73 (SS)	-23.438	-23.331 \pm 0.200	-700.871
Y	81.50	20.1 (Al)	+0.030	+0.066 \pm 0.010	-0.810
Pu	121.55	7.053 (Al)	+8.400	+8.446 \pm 0.020	+69.486
		20.06 (SS)			
U ²³³	146.708	5.286 (Al)	+11.60	11.643 \pm 0.402	+79.362
	(97.15% U ²³³)	19.977 (SS)			

^aSome but not all samples were enclosed in cans of various materials.

TABLE X. Worth of U²³⁵ as Function of Thickness

Number of Samples of Size	Weight, g	Net Worth, lh	Worth/kg, lh
2 x 2 x 0.005 in.			
1	4.511	+0.226 \pm 0.020	50.10 \pm 4.40
2	9.358	+0.401 \pm 0.020	42.85 \pm 2.14
3	13.759	+0.611 \pm 0.020	44.41 \pm 1.45
6	27.628	+1.246 \pm 0.030	45.10 \pm 1.10
12	55.365	+2.493 \pm 0.030	45.03 \pm 0.54
23	105.77	+4.855 \pm 0.010	45.90 \pm 0.10

3. ZPR-9

Spatially dependent reaction rates have been measured with Assembly No. 7 for U^{233} , U^{234} , U^{235} , U^{236} , U^{238} , Np^{237} , Pu^{238} , and B^{10} ; all measurements but the last were determined with the use of small solid-state counters having thin deposits of the fissionable materials on the sensitive surface. The $B^{10}(n, \alpha)$ reaction rate was determined from a small (3/8-in.-dia by 1 1/2-in.-long) high-pressure BF_3 counter.

In addition, the spatially dependent reactivity effects of U^{235} , B^{10} , polyethylene, and borated polyethylene were measured. In these measurements, a probe drive unit was used to move the materials from the core center to the outer region of the radial reflector. Analysis of the reactivity effects was done on-line with the DDP-24 computer. Both types of measurements were made in a 1/2-in.-ID void tube extending vertically in the radial core midplane from slightly below the core center to beyond the reflector edge.

After these measurements were completed, the boron ring experiment was repeated for the Al_2O_3 reflector of Assembly No. 7 in the same manner as was done for the aluminum metal reflector of Assembly No. 6. For the present experiments, however, additional boron was available in the form of powdered crystalline boron (natural) sealed in aluminum cans, 1/8 x 2 x 2 in. There were also available 2500 plates of hot-pressed high-purity B_4C . Variations in empty can weights, packing densities, boron assay, and plate dimensions led to an overall error in the mean of about 5% in the total B^{10} weight.

In order to make a valid computation of the reactivity associated with the boron ring, it was necessary to maintain the same total core leakage and, hence, the same core size as was used in the reference core, Assembly No. 7. For this reason, the reactivity lost because of the boron was compensated by a uniform increase in fuel density. Before the boron was added, Assembly No. 7 had 211.095 kg U^{235} and an excess of 194 lh, a critical radius (corrected for excess reactivity) of 26.94 cm, a length of 51.0 cm, a volume of 116.28 l, and a U^{235} atom density of 0.00451×10^{24} atoms/cm³. With the boron ring (Assembly No. 7C), the critical mass was 257.952 kg U^{235} , including an excess reactivity of 82 lh. The U^{235} atom density in the core was 25% higher except for the central drawer, where it was 50% lower. All other critical parameters were the same.

Spatially dependent reaction rates and reactivity effects were made with the same materials and in the same way in Assembly No. 7C as was done in Assembly No. 7. These data are being analyzed.

Rossi-alpha measurements were made with Assemblies No. 7 and 7C, and will be made again in the same core after the outer reflector and B¹⁰ ring have been removed. In this way, it may be possible to evaluate separately the effects of both slow- and fast-neutron leakage, as well as return currents on the prompt-neutron lifetime.

4. ZPPR

Studies of the gravel samples taken during the coring of the Gravel Gertie test structure are continuing. Eberline and Associates, who performed the coring of the Gravel Gertie structure, has contracted with the Colorado School of Mines Research Foundation Inc., Golden, Colorado, to examine selected samples of gravel to characterize the uranium deposited during the tests. The Research Foundation will also examine a portion of the catenary support structure which was exposed to the effects of the test.

The tests of high-velocity filtration characteristics of the sand portion of the ZPPR gravel-sand roof are continuing. Results of the tests on 12-in. depths of sand, using dioctylphthalate aerosol, show that the minimum efficiency of the sand occurs at a superficial linear velocity of approximately 1 ft/sec.

The following is a status report on reactor components:

Reactor Bed and Tables. The revised drawings of the assembly were reviewed. A visit to the vendor was made to rectify the differences in details between the drawings and the specifications. The main items discussed were the location of the bearings on the movable table and the gear train of the table drive system. Another set of revised drawings is being prepared by the vendor, Giddings and Lewis Machine Tool Co., for submission and approval.

Matrix Drawers. The vendor, Mechanical Products Manufacturing Co. of Seattle, Washington, was visited. There has been some delay in smoothing out the fabrication process. Some preliminary units were made to check the welded ends and the sizing apparatus. The tested welds were satisfactory. It is expected that the vendor will send samples shortly for examination. The inspection and quality control manual is being reviewed.

Matrix Tubes. The four pilot tubes supplied by the vendor, Van Vetter Inc., Seattle, Washington, were not within specifications. ANL personnel visited the Van Vetter plant to review the fabrication method. Apparently, with ample care, the tubes can be fabricated within specification, and the vendor was requested to produce two prototype tubes within specifications and to furnish an inspection and quality control procedure. The prototype tubes and the inspection and quality control manual have been received and are being examined for approval.

Fuel Rod Drives. The holding magnets are now being wound, and the special steel support rods of the drives are being machined. It is estimated that this is 50% complete.

Poison Rod Drives and Reactor Knees. ANL has requested and received extensions of the bid dates from the vendors. These bid awards will be made when the AEC permits further procurements.

Nuclear Instrumentation. Detailed design of the circuitry is proceeding.

D. General Fast Reactor Fuel Development

1. Metallic Fuels

a. Properties of U-Pu-(Ti, Zr) Alloys.

(i) Compatibility. The previously reported excellent compatibility of U-Pu-Zr alloys (see Progress Report for July 1965, ANL-7082, pp. 20-1) with Type 304 stainless steel have been verified by many more tests with both U-18.5 w/o Pu-14.1 w/o Zr and U-15 w/o Pu-20 w/o Zr alloys at temperatures up to 800°C and annealing times to 42 days. Longer-time tests are in progress.

We have also confirmed that alloys very high in nickel (e.g., Hastelloy-X with approximately 50% nickel) are not as compatible, for melting of the reaction products occurs at 750°C with both U-18.5 w/o Pu-14.1 w/o Zr and U-15 w/o Pu-10 w/o Zr in contact with Hastelloy-X.

Incoloy-800 (containing 32% nickel) showed intermediate compatibility. Melting of reaction products occurred at 800°C with U-15 w/o Pu-10 w/o Zr and above 800°C with U-18.5 w/o Pu-14.1 w/o Zr. However, at temperatures below the melting point of the reaction product the occurrence of very extensive penetrations into the fuel and cladding eliminate Incoloy-800 as a useful cladding for U-Pu-Zr alloys.

Compatibility tests are proceeding between U-Pu-Zr fuel alloys and several iron-base superalloys (N-155, Haynes #56, 16-25-6, and 16-15-6).⁵ Preliminary results indicate that N-155 shows no melting of reaction products at 800°C with either U-18.5 w/o Pu-14.1 w/o Zr or U-15 w/o Pu-10 w/o Zr. The N-155 results appear to be similar to those obtained with 304 stainless steel.

⁵N-155 is Fe-0.1 to 0.2 C-18 to 22 Ni-18 to 22 Cr-2.5 to 3.5 Mo-2 to 3 W-0.7 to 1.2 Nb-0.1 to 0.2 N-18 to 22 Co, Haynes #56 is Fe-0.20 to 0.35 C-1.0 to 2.0 Mn-11.5 to 12.5 Ni-10 to 13 Co-20 to 22 Cr-4 to 5 Mo-1 to 2 W-0.7 Nb, 16-25-6 and 16-15-6 are stainless steels containing the indicated amounts of chromium, nickel, and molybdenum. The numbers refer to weight percents.

Work is also progressing on understanding the good compatibility found in the U-Pu-Zr/304 SS system through the determination of an 800°C isothermal section of U-Zr-Fe ternary and U-Zr/Fe diffusion couples. Since the U-Pu-Zr microstructures seem to be particularly sensitive to oxygen impurities, an effort is being made to determine the effect of oxygen content in the fuel on compatibility.

(ii) Compressive Strengths. Compressive strengths of a series of promising metal fuel alloys (see Progress Report for May 1965, ANL-7046, p. 24) containing U-Pu-Zr and U-Pu-Ti have been measured over a range of temperatures (see Table XI). The U-Pu-Zr alloys decrease in strength at room temperature with increasing plutonium content. Zirconium additions strengthen the alloys at high temperature. About one-half the room-temperature strength is retained at 500°C, but at 625 and 675°C the strengths drop off to less than 10% and 5% of the room-temperature values, respectively. Some ductility was observed at 500°C and more at 625°C and above. As-cast and homogenized specimens have similar properties.

TABLE XI. Ultimate Compressive Strength of U-Pu-Zr and U-Pu-Ti Alloys at Selected Temperatures

Alloy (w/o)	Heat Treatment	Ultimate Compressive Strength (kg/mm ²) at				
		25°C	500°C	625°C	675°C	750°C
U-11.1 Pu-6.3 Zr	Hom ^(a)	164	-	12	4.0	-
U-12.3 Pu-14.1 Zr	Hom	166	-	-	6.9	4.2
	As-cast	164	>55	12	5.2	-
U-16.6 Pu-6.3 Zr	As-cast	127	>55	11	2.5	-
U-15 Pu-10 Zr	As-cast	129	48	11	5.6	-
U-18.5 Pu-14.1 Zr	Hom	116	-	-	5.6	-
U-9.1 Ti	Hom	145	115	80	65.0	35.0
	As-cast	150	95	65	50.0	30.0
U-11.4 Pu-3.4 Ti	Hom	96	-	-	6.3	-
U-17.1 Pu-3.4 Ti	Hom	96	-	-	3.8	-
U-15 Pu-6.5 Ti	Hom	130	37	13	6.3	4.2
	As-cast	158	27	12	9.0	-
U-15 Pu-10 Ti	Hom	90	45	20	10.0	7.0
	As-cast	120	40	-	-	-
U-22.1 Pu-11.8 Ti	As-cast	141	55	30	20.0	10.0

(a) Homogenizing heat treatment: 1050°C for one week, oil quench for the alloys with >10 w/o Zr or Ti; and 950°C for one week, oil quench for alloys with <10 w/o Zr or Ti.

The U-Pu-Ti alloys vary in strength more with changes in titanium than in plutonium content. The alloys containing >10 w/o Ti have about 20% of their room-temperature strength at 625°C. The greater strength at higher temperatures in the high-titanium-content alloys is attributed to the U₂Ti-type phase found in this system. The alloys containing smaller quantities of titanium are comparable with the U-Pu-Zr alloys in strength and ductility in compression.

2. Jacket Materials

Appreciable differences have been observed in the creep behavior of different alloy compositions in the V-Ti-Cr system as previously reported (see Progress Report for June 1965, ANL-7071, p. 21). In the light of recently reported room-temperature elastic-modulus values for alloys in this same system, there exists a possible direct relationship between elastic modulus and creep strength. It has been suggested by Sherby⁶ that the creep rate is proportional to the chemical diffusivity and to a function of the elastic modulus, indicating a direct but somewhat complicated relationship between these two parameters.

In the absence of diffusion data for titanium and chromium in vanadium at the testing temperature, an estimate of the relationship between creep strength and elastic modulus is presented in Fig. 13. The modulus

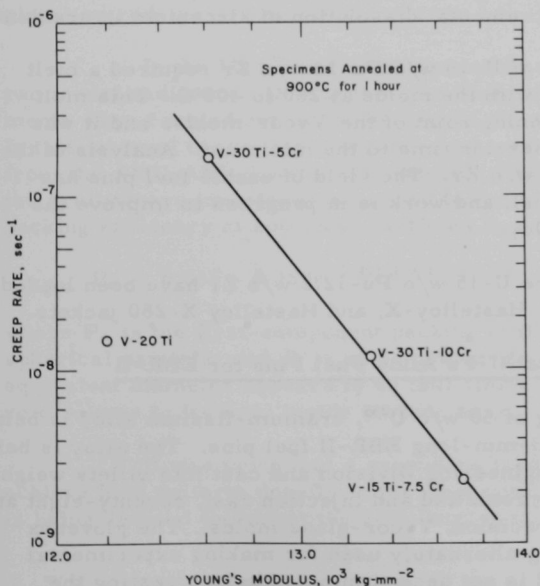


Fig. 13

Creep Rate for V-Ti-Cr Alloys Tested at 650°C and 15 kg-mm² vs. Room-temperature Young's Modulus

⁶Sherby, O. D., Factors Affecting the High Temperature Strength of Polycrystalline Solids, Acta Met., 10, 135 (1962).

values were obtained by use of the equation

$$E_{\text{alloy}} = \sum_i a_i E_i, \quad (1)$$

where a_i is the atom fraction of the i th element and E_i is Young's modulus of the i th element.

The validity of Eq. (1) will have to be tested by obtaining measured values of Young's modulus at temperature for specific alloy compositions. These values will also serve to verify or modify the relationship represented in Fig. 13.

3. Fabrication of EBR-II-type Irradiation Specimens

Thirty alloying and casting melts were made, mostly of uranium-plutonium-zirconium and uranium-plutonium-titanium alloys. The U-15 w/o Pu alloys were found to cast quite easily with the addition of 10 w/o Ti or Zr. The temperatures have been found to be about the same as required for casting uranium-fissium alloys.

Both alloying and injection-casting problems have been experienced in making the U-15 w/o Pu-14 w/o Zr fuel pins. The dissolution of 33 v/o of zirconium in the U-17 w/o Pu alloy required temperatures in excess of 1650°C, and at these temperatures crucible attack was experienced. Better results were made by the incremental dissolution of zirconium in uranium.

The injection casting of U-15 w/o Pu-14 w/o Zr required a melt temperature of about 1550°C with the molds at 260 to 400°C. This melt temperature is near the softening point of the Vycor molds, and it was necessary to reduce the immersion time to the minimum. Analysis of the resulting fuel pins gave 12.2 w/o Zr. The yield of usable fuel pins has tended to be lower than normal, and work is in progress to improve the casting techniques for the alloy.

A total of twenty of the U-15 w/o Pu-12.2 w/o Zr have been loaded; five each into 304 SS, 316 SS, Hastelloy-X, and Hastelloy X-280 jackets.

4. Production of Supplemental U-Fs Alloy Fuel Pins for EBR-II

Approximately 200 kg of 50 w/o U^{235} , uranium-fissium alloy is being cast into 3.66-mm-dia by 343-mm-long EBR-II fuel pins. The alloy is being prepared by the Chemical Engineering Division and cast into billets weighing 6.5 kg. These billets are remelted and injection cast, seventy-eight at a time, into yttria-coated, precision, Vycor-glass molds. The glovebox injection-casting line is being alternately used for making experimental plutonium alloy fuel rods and is not decontaminated before casting the EBR-II fuel pins. The pins are, therefore, alpha radioactive and must be handled as if contaminated with plutonium.

After stripping from the Vycor molds, the castings are visually inspected and cropped to length. The resulting fuel pins are individually weighed and gaged for length, as well as for maximum, minimum, and average diameter.

After inspection, the fuel pins are placed in numbered loops of a vinyl bandolier. The bandolier of pins from a single casting batch are sealed from the glovebox system in lie-flat vinyl pouches and radiographed by means of a Co^{60} source. Radiographic rejects are removed from the bandolier and returned to the glovebox line for remelting. The bandolier with the acceptable pins is then coiled into a compact roll and sealed in a tight-fitting envelope.

By October 18, a total of seventeen injection casting melts had been made and produced slightly more than 1000 visually acceptable castings. The first thirteen melts have been dimensionally inspected, and 751 castings have been vault stored for shipment to Idaho.

5. Carbide Fuels

a. Powder-loaded, Radiator-type Fuel Elements. The term "Radiator Fuel Element" has been given to a concept in which a fuel is loaded into the body of a shell-and-tube type of assembly. Such shapes may afford higher heat-exchange rates and simplified assembly techniques over plate- or rod-type elements.

In the March report reference was made to the construction of two model radiators. During the July-September period, initial experiments were carried out on the loading of the radiator sections with spheres. In this interval twelve experimental runs were made by a team of students from the AMU-ANL Summer Engineering Practice School. The result of the preliminary investigation has led to the following expression for the packing efficiency of spherical particles in a shell-and-tube configuration:

$$P_e = 0.635 - 0.350e^{-0.451 D/d^1},$$

where P_e is the first-component packing efficiency, d^1 the diameter of the spherical particle, and D is an equivalent diameter of the container. The equivalent diameter appears to be four times the ratio of the container void volume to its total inside surface area.

It was found that a secondary mode of vibration was required to achieve high uniform density in the first component. A mechanical system is being devised to impart the additional mode.

Work has commenced on the final phases of the investigation into the compaction of shapes to determine the characteristics of particles and vibration which will yield high uniform densities in the shortest time. Apparatus to study the factors affecting the rate of infiltration of particles was completed.

6. Development of Refractory-metal Alloys for Service in Oxygen-contaminated Sodium

Binary vanadium alloys, carefully prepared by levitation melting to insure homogeneity, have been exposed to 650°C sodium (containing 40-45 ppm O) for one week. The weight changes are given in Table XII.

TABLE XII. Binary Vandium Alloys
Exposed to 650°C Sodium

Oxygen 40-45 ppm	
Nominal w/o of Element in Alloy	Weight Loss, mg/cm ²
10 Aluminum	51.2
10 Copper	104.0
10 Chromium	61.4
20 Chromium	27.5
10 Iron	88.5
20 Iron	91.8
10 Nickel	93.8
20 Nickel	115.0
2 Silicon	82.5
20 Titanium (Controls)	28.8, 28.4

Although some arc-melted binary vanadium alloys were exposed in the initial experiments in this program, no reliable oxygen analyses for the sodium or corrosion evaluation systems were available at that time. The results from this current group of alloys substantiate the earlier conclusion that aluminum, chromium, and titanium are beneficial additions. Micro-examination of the corroded samples to determine internal oxygen penetration has not been completed. Of this group of alloys, only the 20 w/o chromium binary retained a substantial coating of corrosion product after vigorous brushing.

At present, ternary alloys of the series V-40 Ti-X are being exposed to 650°C sodium.

E. General Fast Reactor Fuel Reprocessing Development

1. Skull Reclamation Process

The skull reclamation process is being developed specifically for the recovery of the 5 to 10% of uranium charge that is left in crucibles after melt refining discharged fuel pins from the EBR-II reactor. However, the chemistry and technology developed in this process will also be applicable to the processing of a variety of uranium-bearing fuels.

This process, which has recently undergone modification (see Progress Report for June 1965, ANL-7021, pp. 24-25), consists of initial extraction of the relatively noble fission products into zinc from a suspension of the skull oxides in a halide flux. The zinc phase is then discarded to waste. The uranium oxides are then reduced by magnesium contained in a 60 w/o Mg-Zn reducing solution and the uranium metal precipitates almost completely. Rare earth and alkaline earth elements remain in the flux and supernatant metal phases, which are removed and discarded. The precipitated uranium is dissolved in a Zn-14 w/o Mg solution, and the product solution is cast into an ingot that is subsequently transferred to retorting equipment. In the retorting step, the solvent metals are evaporated, leaving behind a uranium metal sponge which is melted and consolidated into an ingot for recycle to melt refining. This revised process is being tested in plant-scale equipment (~4.25 kg of U per batch) for later installation in the Fuel Cycle Facility at Idaho.

In all, ten plant-scale skull reclamation runs have now been completed. Mechanical operations, viz., charging of materials, heating, mixing, sampling, and transferring molten metals and fluxes from the furnace to exterior receivers, have been performed without difficulty. The rebuilt transfer line (see Progress Report for September 1965, ANL-7105, p. 33) has shown excellent performance in 29 separate phase transfers. The newly designed exhaust manifold, which is attached to the furnace charging port to control fumes that tend to escape during intermediate charging operations (see Progress Report for August 1965, ANL-7090, p. 27), has performed very well. Preliminary analytical data indicate that uranium recoveries will be satisfactory. Cerium removals are also satisfactory, but inadequate removals of molybdenum and ruthenium have been realized, a result that is attributed to inadequate mixing of flux and metal phases. Steps are being taken to provide more vigorous agitation in the crucible.

The final step in the skull-reclamation process consists of retorting, or solvent evaporation, to recover the product uranium from the uranium solution produced in the dissolution step. In this step, the magnesium-zinc-uranium ingot from the skull-reclamation furnace is first transferred to a large beryllia crucible (8½-in. OD by 17-in. overall height by 0.5-in.-thick wall); then the magnesium-zinc is distilled under vacuum at 650 to 750°C

from the uranium product solution. Finally the uranium is melted ($\sim 1200^{\circ}\text{C}$) to form an ingot. Four plant-scale retorting runs (~ 30 kg charge material) have been completed, using Zn-Mg-U ingots which were products of previous skull oxide reclamation furnace runs. Operation of the equipment was satisfactory. Although an isostatically pressed beryllia crucible showed hair-line cracks after two runs, a thixotropically cast beryllia crucible was in good condition after similar usage.

2. Processes for Future Fast Reactor Fuels

Compact pyrochemical processes are under development for processing fast breeder reactor fuels of the ceramic (e.g., oxide or carbide) or metallic types. Such processes utilize Cd-Mg, Cu-Mg, or Zn-Mg solvent alloys in contact with molten halide salts.

A general type of flowsheet based on the selective transport of uranium and plutonium from a Cu-Mg solvent alloy to appropriate Zn-Mg alloys through a chloride salt phase is currently under investigation (see Progress Report for September 1965, ANL-7105, Fig. 12 on p. 34). Because small volumes of metal and salt solutions are required and because separation factors are high, the process is easily adapted to batch separations.

In small-scale (~ 20 g uranium) laboratory experiments, the rate of uranium transfer has been low because little provision has been made for bulk transport of equilibrated salt between the solvent metal phases, other than intermingling of salt eddies above the two metal phases. The process is similar to a Soxhlet extraction in which small increments of solute are transported from a source to a sink phase. In principle, complete transport of a solute element should be achievable in a relatively short time, i.e., less than 24 hr, by circulating or cycling salt between the two metal phases. An engineering-scale experiment is now being set up to demonstrate rapid transfer of uranium from a Cu-Mg phase to an Mg-Zn phase by transferring salt back and forth between vessels containing the metal phases. Between transfers, the salt will be equilibrated with the metal phase by vigorous mixing of the two phases. A conceptual flowsheet for plant-scale processing using the Cu-Mg/salt/Zn-Mg system is shown in Fig. 14.

In this type of process, which utilizes Cu-Mg/molten salt/Zn-Mg, uranium is collected in a Zn-80 w/o Mg alloy, and plutonium in a Zn-2 to 3 w/o Mg alloy. The solubilities of plutonium in these alloys are as follows:

Alloy	Plutonium Solubility (w/o)		
	600°C	700°C	800°C
Zn-2 w/o Mg	0.33	2.33	7.8
Zn-3 w/o Mg	0.28	2.22	8.0
Zn-80 w/o Mg	50.1	49.8	51.8

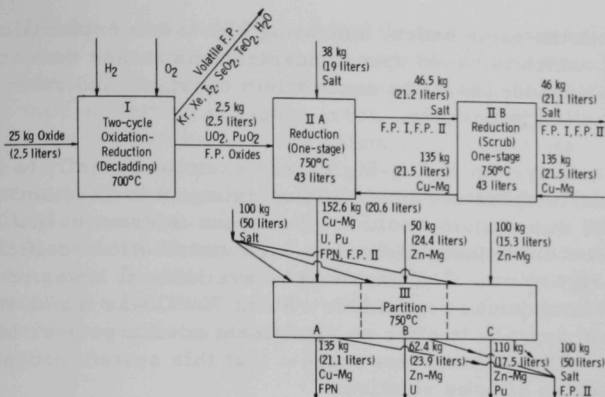
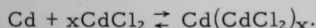


Fig. 14. Conceptual Flowsheet for 1-day Processing of Oxide Fuel from a 1000-MWe Fast Breeder Reactor

Some recent work has also been done on the cadmium-based systems, which have an advantage over other solvent metal systems from the standpoint of corrosion. One of the cadmium-based flowsheets under consideration involves the immediate oxidation of uranium by CdCl_2 to form UCl_3 and cadmium metal. Thus the interaction of CdCl_2 with cadmium metal is of interest.

It has been found that when cadmium chloride in molten salt solutions is used in combination with liquid cadmium, formation of cadmium (I) species may be expected:



Values of x and equilibrium constants K_{eq} for this reaction using LiCl , the LiCl-KCl eutectic, and 50 m/o MgCl_2 -30 m/o NaCl -20 m/o KCl as the molten salt solvent were determined:

Salt	Temperature (°C)	x	K_{eq}
LiCl	650	2.0	0.2
59 m/o LiCl -41 m/o KCl	650	2.2	0.05
59 m/o LiCl -41 m/o KCl	500	2.4	0.01
50 m/o MgCl_2 -30 m/o NaCl -20 m/o KCl	650	1.9	0.3
50 m/o MgCl_2 -30 m/o NaCl -20 m/o KCl	500	2.3	0.08

Although the values of x and K_{eq} have uncertainties of about 20%, it can be concluded that x has a value of 2 in the three solvents, and that at a given temperature K_{eq} decreases in the three salts in the order MgCl_2 - NaCl - $\text{KCl} > \text{LiCl} > \text{LiCl-KCl}$. The activity coefficient of CdCl_2 would be expected

to decrease in the same order, indicating a possible explanation for the variation in K_{eq} , which is based upon concentrations rather than activities. The temperature dependence of the equilibrium constants indicates that the enthalpy of reaction is positive.

The salt system $MgCl_2$ - $MgBr_2$ was examined briefly to determine whether a low-temperature liquid region exists in the system. If such a region exists, this system would be of process interest in that the high magnesium ion concentration, which gives high distribution coefficients (now supplied by $MgCl_2$; m.p. $716^\circ C$), would be available at lower process temperatures. Since no liquidus region below about $700^\circ C$ was found, the $MgCl_2$ - $MgBr_2$ system appears to offer no significant advantage over $MgCl_2$ as a process salt. The observations suggest that this system probably forms a continuous series of solid solutions.

Engineering work related to the development of continuous molten metal-molten salt extraction processes is under way. Initial experiments were designed to permit examination of metal-salt extraction kinetics for transient reactions in packed columns (see Progress Report for August 1965, ANL-7090, p. 28). A 1.4-in.-ID extraction column, which has a 36-in. packed section, is now being used to determine the mass transfer of rare earth elements between countercurrent metal-salt systems under steady-state conditions. In such a countercurrent extraction experiment on the transfer of cerium from a cadmium phase to a chloride salt phase, 88% of the cerium was transferred (material balance 92%). The height equivalent to a transfer stage was about 15 in., which is in excellent agreement with the earlier transient tests. This result is encouraging with respect to the feasibility of metal-salt countercurrent extraction processes.

Four batches (total of 87.5 kg) of salt (50 m/o $MgCl_2$ -30 m/o $NaCl$ -20 m/o KCl) have now been purified in the engineering-scale salt-purification facility (see Progress Report for July 1965, ANL-7082, p. 28). Purification of salts containing $MgCl_2$ is necessary since untreated $MgCl_2$ salts are extremely corrosive toward all steels and contain large quantities of insolubles and substances (particularly water) that react with UCl_3 to form UO_2Cl_2 and UO_2 . The quality of the purified salt, as measured by the content of oxygen and water insolubles, has been steadily improving; the latest batch of salt analyzed <0.1 w/o oxygen and about 30 ppm water. Two salt samples will be submitted to Oak Ridge National Laboratory for fast-neutron activation analysis for oxygen.

3. Materials Evaluation

A new crucible material, "vitreous" carbon, is currently undergoing tests as a container material for liquid metal solutions containing uranium and zinc (see Progress Reports for March 1965, ANL-7028, pp. 33-34 and April 1965, ANL-7045, p. 23). In the latest of such experiments, it was

found that in 200-hr tests at 800°C neither the metal phase of a zinc-2 w/o uranium/salt⁷ nor of a zinc-5 w/o magnesium-2 w/o uranium/salt⁷ system wet the crucible. Wetting by the salt phase appeared, at most, to be very slight. This lack of wetting is highly encouraging in that it is indicative that corrosion of vitreous carbon in these solutions is negligible.

A shear-formed tungsten crucible (11.1-in. OD by 18.1 in. high by 0.18-in. wall thickness) has been received from Metallwerk Plansee, the Austrian affiliate of the National Research Corporation. This is probably the largest tungsten crucible ever fabricated by this technique. The crucible will be thermally cycled, and then its performance for containment of salt and metal systems will be evaluated.

⁷47.5 m/o MgCl₂, 47.5 m/o CaCl₂, 5 m/o MgF₂.

II. GENERAL REACTOR TECHNOLOGY

A. Experimental Reactor and Nuclear Physics

1. Measurements of Small Reactivity in ATSR

Measurements of small reactivity ($<1.5 \times 10^{-5} \Delta k/k$) are being made at the Argonne Thermal Source Reactor (ATSR).⁸ Samples are pneumatically driven through a cadmium-covered tube into the center of the reactor core. The resulting reactivity change is just compensated by an automatically positioned fine-control rod (servo rod) whose movement keeps constant the signal current from a compensated ion chamber, located near the edge of the core. The change in the position of the servo rod is a measure of the reactivity worth of a sample. The reactivity worth per unit change in the servo rod position is determined directly from period measurements.

Gold has been the material studied most extensively in the ATSR to date, both in the amount of data taken and in the variety of sample composition and geometry. Lead was found to be the least objectionable diluent material (with regard to self-shielding) but only few materials of interest

alloy well with lead. Powdered metallurgical techniques using 300-mesh aluminum powder as the diluent material proved unsatisfactory because of the large amount of Al_2O_3 apparently present in the aluminum. A number of chemical analyses indicated varying and unpredictable amounts of water in the aluminum powder. Even the presence of known quantities of oxygen and hydrogen introduces moderately large and statistically uncertain corrections to the data.

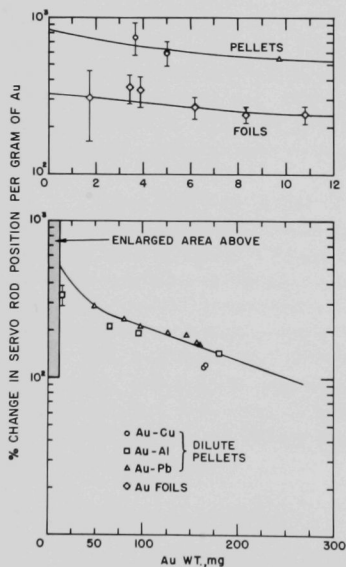


Fig. 15. Reactivity Measurements of Gold

Measurements of the reactivity of gold samples are shown in Fig. 15, in which the logarithm of the percent change in rod position per gram of gold is plotted as a function of the mass of the gold sample. By extrapolation to zero sample mass, $(820 \pm 70)\%$ rod change per gram for dilute pellet samples and $(320 \pm 50)\%$ rod change per gram for thin-foil samples were found. The calibrations of the servo control rod were then found to be 1.893 ± 0.162 b per percent change in rod position per gram

⁸The performance characteristics of ATSR are to be found in Bennett, E. F., and Long, R. L., Nucl. Sci. Eng. 17, 425 (1963).

for dilute pellet samples and 4.850 ± 0.758 b per percent change in rod position per gram for foil samples. This calibration is based upon a value of 1580 b for the infinite-dilution absorption integral of gold from which 28 b was subtracted to account for the higher effective cadmium cutoff energy in reactivity measurements.⁹

The servo rod calibration can be used to convert reactivity measurements on samples into effective absorption integrals provided the rod position varies linearly with reactivity (this has been checked from time to time) and the reactivity varies directly with the effective absorption integral of the sample (if not, an importance weighting correction should be applied).

Results are given in Table XIII. Enough data were taken for different sample dilutions so that crude extrapolations could be made to the case of infinitely dilute samples. The infinite-dilution absorption integrals in Table XIII have not been corrected to a standard value of cadmium cutoff energy nor has any correction been made for importance weighting which may differ from that of the gold. The large spread in the infinite-dilution values results from the uncertainties in extrapolating to zero sample mass, which can be appreciated by comparing columns 2 and 3 of Table XIII. The uncertainties can be reduced by taking data for more dilute samples.

TABLE XIII. Absorption Integrals Extrapolated to Infinite Dilution

Sample	% Rod Change per Gram of Sample		Infinite-dilution Absorption Integral, b	Form of Sample ^a
	For Lightest Sample Measured	Extrapolated to Zero Sample Mass		
Gold	740 ± 180 (3.5 mg)	820 ± 70	1580 ^b	Machined pellets of Au/Cu and Au/Pb alloy; pressed powder with Al diluent.
Indium	424 ± 7 (91.4 mg)	1500 ± 300	2840 ± 618	Machined In/Pb alloy pellets.
Silver	447 ± 32 (23.41 mg)	600 ± 140	1136 ± 282	Pressed powder with Al diluent.
Cobalt	414 ± 43 (14.12 mg)	800 ± 300	1517 ± 583	Pressed powder with Al diluent.
Gold	310 ± 150 (1.77 mg)	320 ± 50	1580 ^b	Au foil of 1.016-cm dia.
U ²³⁸	10.47 ± 0.23 (2.089 mg)	55 ± 20	267 ± 106	U foil, hollow cylinder.

^aPellet samples were of 1.016-cm dia and from 0.45 to 1.27 cm long.

^bKnown value used to calibrate the servo rod.

⁹Brown, H. L., Jr., and Connolly, T. J., Trans. Am. Nucl. Soc. 6, 236 (1963).

2. High Conversion Critical Experiments (Hi-C)

A cylindrical core of aluminum-clad Hi-C fuel pins was loaded to critical in a 1.349-cm (0.531-in.) square-pitch lattice. This core had an atomic ratio of hydrogen to U^{238} of 4.15 and is the loosest uniform-lattice core yet assembled with the Hi-C fuel. Measurements performed in this core will allow an overlap between the Hi-C data and the data obtained with similar fuel at other laboratories¹⁰ in the range of atomic ratios of hydrogen to U^{238} from 3 to 5.

The clean, control-rod-free, fully reflected critical loading for this core was 589 ± 2 fuel pins, corresponding to a U^{235} critical mass of 13.48 ± 0.04 kg and a clean, critical core radius of 18.47 ± 0.03 cm.

Each of the finger-type control rods had a worth of $0.67\% \Delta k/k$ at the core periphery, and the blade-type control rods had a total worth of $1.05\% \Delta k/k$ at the core periphery. The peripheral fuel pin within a core of average radius 18.8 cm was found to be $0.025\% \Delta k/k$ per pin.

Radial and axial activation traverses are in progress to determine reflector savings and critical buckling.

B. Theoretical Reactor Physics

1. Effects of Randomness on Group Cross Sections

Previously reported work on effective cross sections of Pu^{239} (see Progress Report for September 1965, ANL-7105, pp. 40-41) referred only to cross sections averaged over small (200 eV) energy ranges. To make a realistic calculation of the effects of randomness on reactivity coefficients 26-group flux and adjoint flux calculations were made for a bare sphere of the composition used in the fine-group analysis. Bondarenko's 26-group set¹¹ was used. The relative changes in Pu^{239} fission and absorption cross sections in going from 300 to 600°K were calculated for each of 26 broad groups by weighting the corresponding fine-group changes with the associated energy span; where resolved data were available, the broad-group shift was calculated directly. Assuming a correlation coefficient of 0.7 between $\delta\Sigma_a/\Sigma_a$ and $\delta\Sigma_f/\Sigma_f$, we estimated the variance in the Doppler shift for each group and the variance for the total energy range. The value of 0.7 was computed for the typical interval of 700 to 900 eV and was assumed constant for the entire range from 200 to 10,000 eV.

¹⁰Hellens, R. L., and Price, Glenn A., Reactor-physics Data for Water-moderated Lattices of Slightly Enriched Uranium, Reactor Technology--Selected Reviews, TID-8540 (1964).*

¹¹Bondarenko, I. I., ed., Group Constants for Nuclear Reactor Calculations, Translated, Consultants Bureau, New York (1964).

In Table XIV the nonzero contributions to the Pu^{239} Doppler shift are listed by group, including the weight $w_g = \delta \nu \Sigma_f$ of each group, the relative cross-section changes $\delta \Sigma_f / \Sigma_f$ and $\delta \Sigma_a / \Sigma_a$, as well as their variances, the weighted contribution to the reactivity change, $w_g(\delta k/k)_g$, and the variance in $(\delta k/k)_g$, namely, V_g .

TABLE XIV. Contribution to Pu^{239} Doppler Coefficient

Group No.	Lower Bound, eV	$w_g = \phi_g \nu \Sigma_{f,g}$ ($\times 10^3$)	$\delta \Sigma_f / \Sigma_f$ ($\times 10^3$)	$\delta \Sigma_a / \Sigma_a$ ($\times 10^3$)	$w_g(\delta k/k)_g$ ($\times 10^3$)	V_g ($\times 10^6$)
12	4650	4.849343	0.894	0.824	0.0272	21.64
13	2150	1.700301	2.756	2.38	0.0296	144.9
14	1000	4.536167	6.148	6.346	0.1492	14.35
15	465	4.308070	6.002	6.644	0.1016	19.26
16	215	3.514656	2.755	5.186	-0.0135	18.91
17	100	2.065059	32.547	39.048	0.1935	Resolved Resonances
18	46.5	1.256328	61.521	64.734	0.2055	Resolved Resonances
19	21.5	0.208488	64.089	105.637	-0.0030	Resolved Resonances
20	10.0	0.193010	63.481	74.234	0.0353	Resolved Resonances

The conclusion is that $(\delta k/k)_{49} = (0.730 \pm 0.29) \times 10^{-3}$; the error is the probable error based on the variance of the unresolved contributions only. The contribution to $(\delta k/k)_{49}$ from the unresolved resonances is 0.290×10^{-3} . The large contribution from the resolved resonances comes from recently reported data which include resonances with extremely large (about a few eV) fission widths.

2. The Argonne Reactor Computation System (ARC)

Reactor problems have been attacked by using a number of self-contained and unrelated computer codes, each having unique input requirements and furnishing results on a variety of output media, such as printed page, tape, and punched cards. Problems requiring the application of several such codes, with results of one code used as input for another, normally involve several unrelated computer runs with intervening manipulation of data.

The Argonne Reactor Computation System (ARC), which is intended for use on a next-generation computer, represents a break with such methods in all respects. Although the determination of specific details concerning the system must await information concerning the exact machine configuration involved, the general features of ARC can be described (see Fig. 16).

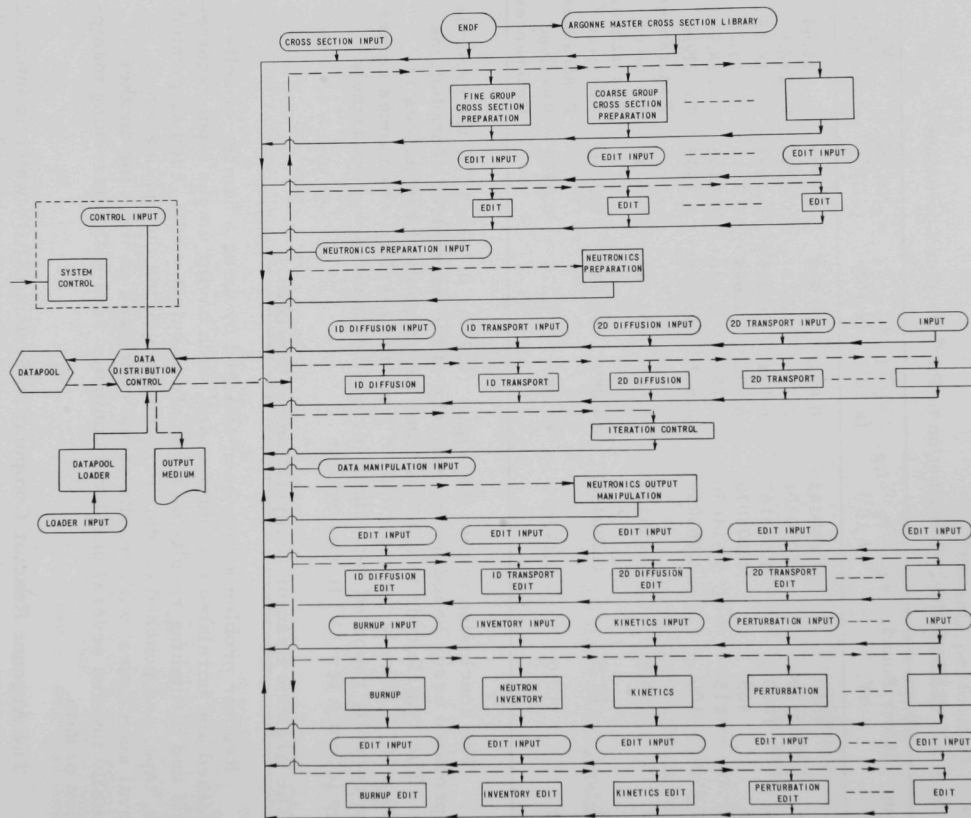


Fig. 16. Schematic Representation of ARC

The ARC System consists of a collection of modular computation units which operate under the direction of a central SYSTEM CONTROL (SC). The SC has a variety of functions, such as

- (a) specifying the route to be taken through ARC;
- (b) specifying conditions for alternative routes and exits;
- (c) specifying the destiny of the data generated by the current ARC run.

The SC is a FORTRAN program generated at run time. Thus, there is no limit to the complexity of the route to be taken through ARC other than that imposed by the ingenuity of the user. The CONTROL INPUT (CI) consists of a series of FORTRAN statements which, when compiled, will become the SC. The CI also contains certain alpha-numeric data which identify the problem to be run and supply other information to the SC for use in the various functions listed above.

Individual computation modules are restricted in scope so that, for example, the neutronics modules such as 1D Diffusion and 2D Transport, are concerned only with the algorithms involved in computing fluxes, k_{eff} , etc. They are specifically not involved in manipulating input or output.

The neutronic modules are standardized with regard to their interface quantities. In particular, the adjunct codes, which depend to a large extent on data generated by the neutronics modules, will be compatible with any of these modules. Thus, for example, only one Neutron Inventory module is required for ARC rather than one for each different type of neutronics module.

Once the interfaces are defined for any of the computation modules in ARC, programming of that module can proceed without knowledge of other modules of the system. This aspect is extremely important in that it permits programming and assembling a limited ARC which can be put into use while further subsequent modules are being developed.

This independence of the various computational modules is made possible by use of the DATAPOOL concept. The ARC uses a DATAPOOL with all external inputs as well as the results generated by all of the computational modules being stored in the DATAPOOL under the direction of the DATA DISTRIBUTION CONTROL (DDC). Similarly, all of the data which any module may require are supplied to that module by the DDC from the DATAPOOL. (A DATAPOOL concept is working on the CDC-3600 with a system concerned with nuclear shell-model calculations.)

The DATAPOOL can be loaded at run time by means of the DATAPOOL LOADER (DL). The DL can be used to supply some data which

normally would be generated by a computation module. The DL also facilitates rerunning problems with very few parameter changes.

The DDC will be able to locate specific blocks within a given superfile and will be able to locate a given superfile which was loaded into the DATAPOOL at some earlier time. The DDC will also be used in conjunction with the DL to generate a new superfile with specific changes being supplied by the DL.

The programming of individual computation modules can proceed using FORTRAN IV, following specification of the interface quantities. Testing of individual modules can be done with the CDC-3600 or IBM-704 even before the new machine is available.

As indicated on the schematic figure, the ARC System is open-ended and can be extended indefinitely. Thus, at the neutronics module level, further modules might include a fundamental-mode calculation, an integral transport solution to the Boltzmann equation, a Monte Carlo calculation, 3D diffusion theory, etc. At the adjunct module level, further modules would include a spatial synthesis module for facilitating generation of input for multidimensional neutronics computations, a hydrodynamics calculation, a cost-analysis calculation, a group-collapsing routine, etc. In addition, a general FORTRAN compilation capability will be included so that the user may generate an adjunct module at run time.

3. Development of Reactor Computing Codes

The Argonne version of the space-dependent multigroup thermalization code THERMOS has been modified to correct an error and an oversight. An error was made in preparing an overlaid version of the code for use with the CDC-3600 computer. An oversight occurred when the code was used to generate a pseudo-material for use in a subsequent problem. When generating the new material, the scattering kernel was not being transmitted.

Since a rather large amount of data is generated with the pseudo-material option, the original plans to supply a punched-deck output have been abandoned. Instead, the pseudo-material cross sections are now written in binary on tape. In order to run a problem at a later date using this data, the user must request that the tape be saved. For input to a subsequent run, the tape must be remounted in the machine. When sequential problems occur during the same run, the tape handling is automatic as before.

4. Evaluation of Cross Sections

A study of the effects of the use of multilevel cross sections in the case of fissionable isotopes is being carried out. A FORTRAN code,

MUFFLE,¹² which calculates multilevel cross sections according to Vogt's formulation,¹³ has been obtained and adapted to the CDC-3600 computer. MUFFLE was used to calculate cross sections for two nearby resonances having the same Γ_n , Γ_f , Γ_γ , and various angles between their fission vectors.¹³ The value of $\alpha = \Gamma_\gamma/\Gamma_f$ varies rapidly as a function of energy unless the fission vectors are almost perpendicular. If the two resonances are fairly well-spaced, the ratio $\bar{\alpha}$ of the infinite-dilution capture and fission integrals is roughly equal to the common value of Γ_γ/Γ_f , but for small spacings $\bar{\alpha}$ decreases considerably when fission vectors are nearly parallel and increases considerably when they are nearly antiparallel.

It is well-known that use of single-level resolved resonance parameters to calculate $\bar{\alpha}$ for U^{235} yields a value of the order of 1.0, whereas experimental measurements of infinite-dilution resonance integrals give $\bar{\alpha} \approx 0.5$. MUFFLE is to be used to generate multilevel cross sections and then attempt to fit them with single-level formulae. For this purpose several FORTRAN codes have recently been written and tested. These include a code to generate input to MUFFLE according to statistical distributions, and single-level, least-squares-fit codes to derive resonance parameters from fitting both total and fission cross sections.

C. High-temperature Materials Studies

1. Ceramic Fuel Materials

a. Thermal Stability. Work was continued on a program aimed at the evaluation of the thermal behavior of plutonium ceramics in various atmospheres.

A glovebox TGA apparatus is being tested. The furnace was heated to 2200°C with a tantalum element in vacuum, and all systems appeared to function properly. A tungsten mesh element is being installed to permit operation at higher temperatures in reducing atmospheres.

(i) (Th-U-Pu)S Bodies. A preliminary study on the oxidation of US was continued. A gas chromatograph is being used to get oxidation rate data. The chromatograph is set up to measure the change in composition of a helium-oxygen stream due to oxidation of a specimen.

The chromatograph calibration is linear over the range from 0.087 to 10.5 v/o oxygen. The calibration was checked by oxidizing

¹²Preskitt, C. A., MUFFLE--A Code for the Multilevel Analysis of Neutron Cross Sections, ORNL-TM-1180 (April 1965).

¹³Vogt, E., Resonance Theory of Neutron Cross Sections of Fissionable Nuclei, Phys. Rev. 112, 203-214 (1958).

a copper specimen at 600°C in He-0.375 v/o O₂. The gravimetrically determined weight gain of 6.2 ± 0.1 mg agreed with that calculated from the chromatograph record (6.06 mg).

The specimens being used for the oxidation runs are US pellets sintered to 85% of X-ray density. Analysis of the gaseous oxidation products from a specimen oxidized at 700°C in He-0.375 v/o O₂ showed that SO₂ was a reaction product. A SO₂ remover, containing MnO₂, was installed to eliminate the interference of this product with the oxygen analysis.

The results of an attempt to determine an oxidation rate on a pellet reacted at 700°C in He-0.375 v/o O₂ indicated that, at a gas flow rate of 100 cc/min, the oxygen supply was completely consumed by the specimen. After this run, a yellow deposit was found on the cooler parts of the furnace tube. This deposit appeared to be sulfur, an indication that the reaction products include free sulfur in addition to SO₂.

A specimen oxidized at 700°C in He-10.5 v/o O₂ ignited almost immediately after the reactive atmosphere entered the furnace tube. The same specimen was cooled to 500°C in pure helium, and another attempt to obtain a rate curve was made. The chromatograph record showed a drop in oxygen consumption for 10 min followed by an abrupt increase, indicating that self-heating had again caused ignition.

b. U-S-O System. It is difficult to produce US shapes that are free of oxygen contamination, which manifests itself as UO₂, UOS, or mixtures of the two. This contamination can have considerable effect on fabrication and properties. A predominance of UOS produces a very fluid, intergranular eutectic liquid that can greatly aid the sintering process and, in excess, can promote deformation; but UO₂ generally persists as inert discrete particles. These structure types are reflected in high-temperature mechanical properties. Bodies containing UOS are fairly ductile although less strong than those containing UO₂, which exhibits brittle behavior. In order to better understand and to predict the behavior of oxygen-bearing phases in US bodies, work has been initiated to study phase relations in the system U-S-O, this research being limited to the U-UO₂-US₂ portion of the ternary. The US-UO₂, US-UOS and UO₂-UOS joints are of prime interest.

Initial efforts in this study have been directed towards the best means of obtaining or preparing the starting materials, which include U, US, US₂, UOS, UO₂, and U₃O₈. An attempt was made to prepare UOS by the oxidation of US powder at low temperatures and oxygen pressures. Only what appeared (in powder patterns) to be a very poorly crystalline UO₂ was obtained at temperatures up to 400°C and oxygen pressures ranging from 2 to 90 mm, but the manner of structure change and excessive weight gain of the powder prompted a more careful investigation.

Over a period of weeks, US powder of carefully analyzed composition was oxidized slowly in air from room temperature to 750°C (reaction with nitrogen is negligible at these temperatures). The progress of oxidation was followed by means of weight change, X-ray powder patterns, and analysis of total oxygen content. From the information obtained, the weights of sulfur and oxygen relative to uranium were determined at all stages of oxidation.

It was found that up to 0.2 atom of oxygen per atom of uranium went into the US structure before any sulfur was lost. As more oxygen went into the structure, sulfur was gradually lost up to the point where, at 500°C, 0.5 atom of sulfur and 3.0 atom of oxygen were present per atom of uranium. It appears that the oxygen was taken interstitially into the US rock-salt structure (with almost no change in lattice parameter) until enough oxygen was present to stabilize a strained UO_2 fluorite structure (having only a slightly smaller lattice parameter than US) with the sulfur as the interstitial phase. At temperatures over 480°C U_3O_8 was formed (with retained sulfur), and at around 700°C the entire residual sulfur content was lost and a sharp U_3O_8 pattern was obtained.

Considerable amounts of oxygen can be taken into the US structure without being readily detected either visibly or with X rays. This occurrence of oxygen could very possibly account for the fact that chemical analyses have often shown more total oxygen content than could be accounted for by the amount of oxygen determined to be in the UOS and UO_2 phases.

c. Anelasticity of Some Uranium Compounds. The elastic modulus of stoichiometric uranium oxide at room temperature increases with increasing density. When the volume fraction porosity is smaller than 0.1, either linear or exponential equations can be used to calculate the elastic characteristic as a function of density. When the volume fraction porosity becomes larger than 0.1, a linear equation seems to be the most suitable. The linear expression is given by

$$E = 2233.85(1 - 2.277P)$$

and the exponential equation by

$$E = 2243.56e^{-2.52P}, \quad (4)$$

where E is the elastic modulus of porous polycrystalline uranium oxide and P is the volume fraction porosity.

The elastic modulus of stoichiometric nonporous uranium dioxide at room temperature was found by extrapolation to be 2243.56 ± 22.1 kilobars when using the exponential equation and 2233.85 ± 22.05 kilobars when employing the linear expression (see Progress Report for September 1965, ANL-7105, p. 42). Internal friction of UO_2 decreases sharply

as the grain size increases. Other microstructural characteristics, namely, number, size, and position of pores also contribute to this behavior. In nonstoichiometric urania the presence of a second phase is the pre-eminent factor dictating the damping properties at room temperature.

Young's modulus for nonstoichiometric uranium oxide depends mainly on the history of the sample. Varying the oxidation and/or the rate of cooling will produce completely different results.

When studying or specifying the elastic or anelastic characteristic of nonstoichiometric urania, one must characterize the material not only by the oxygen-to-uranium atom ratio, but also by microstructure, particularly the number, location, and quantity of solid phases present.

In the oxidation range studied here the ratio of UO_{2+x} to U_4O_9 (or U_4O_{9-y}) is needed to relate properties or uranium-oxygen content.

d. Development of Thermal Diffusivity Apparatus. Additional work on PuS (see Progress Report for September 1965, ANL-7105, p. 39) as well as an initial run on PuP were carried out. The results are shown

SYMBOL	COMPOUND	DENSITY % THEOR	W/O OXYGEN	W/O NITROGEN
○	Pu S	88.2	0.03	0.03
○	Pu S	93.0	0.20	0.05
●	Pu P	88.2	0.05	0.02

in Fig. 17. Even though the PuS batch with the higher oxygen content sintered to a higher density, its thermal diffusivity was found to be equal to only half that of the high-purity material. It is believed that a second phase seen in photomicrographs of the low-purity material was responsible for its lower thermal diffusivity.

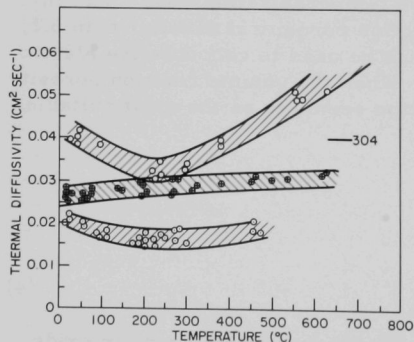


Fig. 17. Thermal Diffusivity of Plutonium Compounds

The dip in the diffusivity of PuS between 200 and 300°C may be due to changes in the contribution of the electrons to the total thermal conductivity. Work on the electrical conductivity and thermoelectric power of plutonium compounds is in progress and will be of aid in explaining the behavior of the thermal diffusivity as seen in Fig. 17.

It is noted that PuS shows a slightly higher thermal diffusivity than PuP of equal purity. A different trend has been noted in uranium compounds, for which the thermal conductivity increases as the anion changes from Group VI to IV. Additional work on plutonium compounds may reveal an analogous relationship.

The values for the uranium and plutonium monosulfides are similar over the same temperature range. However, the value of the thermal diffusivity of uranium monophosphide was approximately twice that found for the corresponding plutonium compound. It must be emphasized that all the data presented are of a preliminary nature and that small variations in physical and chemical properties may have a large effect on the thermal diffusivity.

e. Thermodynamic Studies of Hypostoichiometric Urania at High Temperatures. The accumulation of fission product elements during fission of urania at high temperatures and/or within steep temperature gradients results in local environments which are chemically oxidizing or reducing. When reducing conditions prevail, hypostoichiometric urania (UO_{2-x}) and/or uranium metal can be formed. Knowledge of the relation between oxygen partial pressure and the stoichiometry of urania at high temperatures will be extremely useful in understanding and predicting the changes in stoichiometry of urania that occur during fission. Accordingly, transpiration measurements of the total pressure of uranium-bearing species and, simultaneously, of the partial pressure of oxygen over hypostoichiometric urania have been made as a function of urania composition. The measurements were conducted with H_2 - H_2O buffering carrier-gas mixtures which served to fix the oxygen partial pressures and thereby control the composition of the solid urania phases. Oxygen partial pressures were calculated from the moisture content of the exit carrier-gas streams. The uranium content of the solid phases and of the uranium-bearing gaseous species (collected on a tungsten condenser) were determined by conventional analytical methods.

Figure 18 shows the results of measurements of (monatomic) oxygen partial pressure over hypostoichiometric urania between 2300 and 2600°K. Included are oxygen partial pressures estimated from the low-temperature (1000 to 1300°K) partial molar enthalpy and entropy values of Markin and Bones¹⁴ for stoichiometric and hyperstoichiometric urania. The oxygen partial pressures corresponding to the hypostoichiometric phase-boundary compositions were calculated by the equation obtained by Ackermann, Chandrasekharaiah, and Rauh¹⁵ in their effusion and mass-spectrometric studies of the urania-liquid uranium two-phase system. The hypostoichiometric phase boundary compositions are from the phase diagram presented by Martin and Edwards.¹⁶ The trend in oxygen partial

¹⁴Markin, T. L., and Bones, R. J., The Determination of Some Thermodynamic Properties of Uranium Oxides with O/U Ratios between 2.00 and 2.03 Using a High Temperature Galvanic Cell. Part II., AERE-R-4178 (Nov 1962), pp. 23 and 24.

¹⁵Ackermann, R. J., Chandrasekharaiah, M. S., and Rauh, E. G., ANL-7048 (in preparation).

¹⁶Martin, A. E., and Edwards, R. K., J. Phys. Chem. 69, 1788 (1965).

pressures obtained via the transpiration method appears to be consistent with expectations, namely, a rapid variation of oxygen partial pressure with composition as the stoichiometric composition is traversed. The experimental partial pressure values for oxygen shown in Fig. 18 are approximately 200 times lower than the values reported by Aitken, Brassfield, and Fryxell.¹⁷ Possibly, equilibrium was not reached in their experiments because relatively high flowrates of carrier gas were used (~4 liters/min as compared to ~1/8 liter/min in this work).

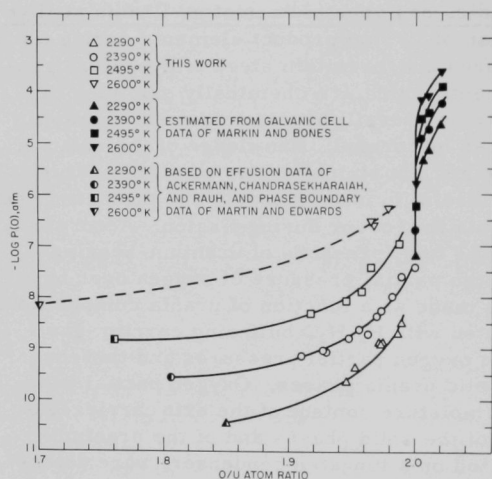


Fig. 18.
Monatomic Oxygen Partial Pressure as a
Function of Urania Composition

Figure 19 shows the results of measurements of the total vapor pressure of uranium-bearing species over urania. The results are

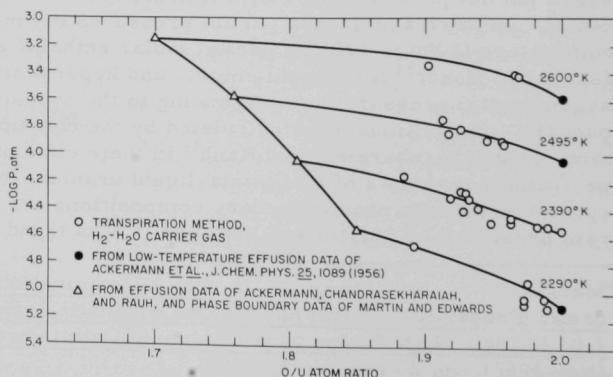


Fig. 19.
Total Pressure of Uranium-
bearing Species as a Func-
tion of Urania Composition

¹⁷Aitken, E. A., Brassfield, H. C., and Fryxell, R. E., Symposium on Thermodynamics with Emphasis on Nuclear Materials and Atomic Transport in Solids, IAEA, Vienna, Austria, July 22-27, 1965, SM-66/83.

consistent with the expected trend of an increase in total pressure of uranium-bearing species (primarily owing to the rapid increase in P_{UO}) as the condensed UO_2 phase is reduced toward the hypostoichiometric phase boundary. Between 2300 and 2600°K, a 2.5- to 3.5-fold increase in pressure of uranium-bearing gaseous species occurs on going from UO_2 to the hypostoichiometric phase boundary, whereas the oxygen partial pressure decreases by several orders of magnitude.

Some vaporization measurements were made over stoichiometric urania. The experimentally determined total pressure of uranium-bearing species over UO_2 at 2390°K was found to be in excellent agreement with the value derived from the extrapolated low-temperature effusion measurements of Ackermann *et al.*¹⁸ The oxygen partial pressure measured at this composition and temperature was approximately fifty times lower than that estimated by extrapolation of the low-temperature thermodynamic data of Markin and Bones.

Work to extend the temperature and composition range of the transpiration measurements is in progress.

2. Liquid-metal Corrosion

a. Polarization Studies. Current effort is aimed at verifying the effect of polarizing current on the thickness of corrosion film, previously observed. Techniques have been improved to: (a) eliminate apparent thin spots in the corrosion film on zirconium, associated with pickup of moisture impurity, and (b) reduce scatter in weight-change data for both polarized and unpolarized samples.

Five zirconium electrodes were exposed together overnight in oxygenated sodium at a central temperature of 580°C to form an electrode-surface corrosion film suitable for subsequent polarization experiments. Weight gains varied only $\pm 8\%$, a significant improvement over previous results. None of the film-spot phenomena associated with moisture was evident. Individual samples of this group are being subjected separately to further exposure at 400°C (central), under either unpolarized or anodically polarized conditions. Polarization voltages of greater than 100 mV have been achieved, throughout a test, across the corrosion film at 400°C with a surface current density of 10 mA/cm². Voltage values are not yet predictable from sample to sample.

The mechanism of film blemishing by sodium-moisture reaction product, i.e., whether film growth is generally inhibited, or the effect is more direct and localized to near the apparent, thin spot areas, has been

¹⁸Ackermann, R. J., Gilles, P. W., and Thorn, R. J., *J. Chem. Phys.* **25**, 1089 (1956).

questioned (see Progress Report for September 1965, ANL-7105, p. 44). Subsequent comparison of weight-gain data of zirconium samples with and without film spots supports the latter view. It is recognized, however, that absorption of hydrogen or oxygen impurity by the sample electrodes at 540°C may interfere with the resolution of the question by comparison of weight-gain data.

Further observations have been made of helium gas impurity levels and their effect on handling alkali metals in two gloveboxes (see ANL-7105, p. 44). A moisture concentration of 6 ppm and an oxygen concentration of less than 1 ppm were measured in helium from a cylinder of BuMines Grade A Helium. Other workers report the moisture level to be frequently higher. Glovebox concentrations of moisture in helium rise to much higher values unless the gas is continually circulated through a dryer. Continuously dried gas has displayed a typical moisture level of 2 ppm (with levels as low as 1 ppm). Sodium may be cut, weighed, and otherwise handled as necessary in this environment without developing a noticeable surface film in the 15-20 min employed. In cooperation with Wang and McFall, it was shown that sodium develops an obvious film almost immediately in helium whose moisture content is on the order of 100 ppm, while lithium appears relatively bright in the same environment after extended time of exposure.

3. Irradiation of Materials for Fast Reactors

The Laboratory's program on irradiation of fast reactor materials includes metallic and ceramic fuels in various fuel jacket alloys, and test specimens of the jacket alloys themselves. The reactors being used for the irradiations include CP-5, MTR, and EBR-II.

a. Metallic-fuel Irradiations. Irradiations presently under way are shown in Table XV. A total of forty-six specimens are under irradiation. The specimens being irradiated in CP-5 are from 4 to 6 in. (10 to 15 cm) long and are in instrumented capsules. Those in MTR are full-length EBR-II size (18 in., 46 cm long) and are in instrumented temperature-controlled capsules. The specimens in EBR-II are also full-length and are located in three special subassemblies. Most of the fuel alloys presently under irradiation are of the uranium-plutonium-fissium type because of their relevance to the EBR-II pyrometallurgical reprocessing cycle. More recently, greater interest has developed in high melting U-Pu-Zr and U-Pu-Ti alloys of uranium and plutonium. Specimens of these alloys will replace most of the fissium-type alloys in the irradiation program.

The CP-5 reactor has been shut down for approximately three months for modifications of the experimental facilities and of the reactor itself. During this shutdown period, the irradiation capsules in the reactor were removed for interim examination of the specimens by neutron radiography. All capsules contain plutonium alloy specimens.

TABLE XV. Status of Metallic-fuel Irradiations in Progress

Specimen No.	Reactor	Fuel Composition, w/o	Clad Composition, w/o	Clad ID, in.	Clad Thickness, in.	Maximum Clad Temp, °C	Calculated Burnup to Date	
							a/o	(t/cm ³) x 10 ⁻²¹
N-15	CP-5	U-19 Pu-14 Zr	V-20 Ti	0.175	0.015	600	4.2	1.4
ND-23	EBR-II	U-15 Pu-10 Zr	V-20 Ti	0.177	0.016	540	0.39	0.10
ND-24	EBR-II	U-15 Pu-10 Zr	V-20 Ti	0.177	0.016	540	0.39	0.10
N-14	CP-5	U-15 Pu-10 Ti	V-20 Ti	0.173	0.015	560	4.6	1.7
NC-17	EBR-II	U-15 Pu-10 Ti	V-20 Ti	0.177	0.016	540	0.39	0.10
NC-23	EBR-II	U-15 Pu-10 Ti	V-20 Ti	0.177	0.016	540	0.39	0.10
N-10	CP-5	U-10 Pu-10 Fz	V-20 Ti	0.165	0.016	540	4.0	1.5
N-11	CP-5	U-10 Pu-10 Fz	V-20 Ti	0.161	0.016	540	4.0	1.5
N-12	CP-5	U-10 Pu-10 Fz	V-20 Ti	0.157	0.016	540	4.0	1.5
CK-01	MTR	U-10 Pu-10 Fz	Nb-1 Zr	0.156	0.015	555	3.1	1.2
CG-02	EBR-II	U-10 Pu-10 Fz	Nb-1 Zr	0.156	0.009	440	0.23	0.087
CG-03	EBR-II	U-10 Pu-10 Fz	Nb-1 Zr	0.156	0.009	440	0.21	0.080
CJ-01	EBR-II	U-10 Pu-10 Fz	Nb-1 Zr	0.156	0.009	435	0.18	0.068
PB-02	EBR-II	U-10 Pu-10 Fz	Nb-1 Zr	0.156	0.009	440	0.20	0.076
TC-1	CP-5	U-15 Pu-10 Fz	Nb-1 Zr	0.156	0.009	550	1.3	0.30
C-152P	CP-5	U-15 Pu-10 Fz	Nb-1 Zr	0.156	0.009	550	1.3	0.30
C-153P	CP-5	U-15 Pu-10 Fz	Nb-1 Zr	0.156	0.009	550	1.3	0.30
C-155P	CP-5	U-15 Pu-10 Fz	Nb-1 Zr	0.156	0.009	590	1.3	0.30
C-156P	CP-5	U-15 Pu-10 Fz	Nb-1 Zr	0.156	0.009	590	1.3	0.30
C-159P	CP-5	U-15 Pu-10 Fz	Nb-1 Zr	0.156	0.009	590	1.3	0.30
N-1	CP-5	U-15 Pu-10 Fz	V-20 Ti	0.157	0.016	575	5.7	2.2
N-2	CP-5	U-15 Pu-10 Fz	V-20 Ti	0.157	0.016	575	5.7	2.2
N-3	CP-5	U-15 Pu-10 Fz	V-20 Ti	0.165	0.016	575	5.7	2.2
N-4	CP-5	U-15 Pu-10 Fz	V-20 Ti	0.161	0.016	575	5.7	2.2
N-5	CP-5	U-15 Pu-10 Fz	V-20 Ti	0.161	0.016	575	5.7	2.2
N-6	CP-5	U-15 Pu-10 Fz	V-20 Ti	0.169	0.016	575	5.7	2.2
N-7	CP-5	U-15 Pu-10 Fz	V-20 Ti	0.165	0.016	540	4.0	1.5
N-8	CP-5	U-15 Pu-10 Fz	V-20 Ti	0.157	0.016	540	4.0	1.5
N-9	CP-5	U-15 Pu-10 Fz	V-20 Ti	0.157	0.015	540	3.1	1.2
CE-03	MTR	U-15 Pu-10 Fz	Nb-1 Zr	0.156	0.015	555	3.1	1.2
EC-01	MTR	U-15 Pu-10 Fz	V	0.156	0.015	555	3.1	1.2
CA-01	EBR-II	U-15 Pu-10 Fz	Nb-1 Zr	0.156	0.009	450	0.22	0.083
CB-02	EBR-II	U-15 Pu-10 Fz	Nb-1 Zr	0.156	0.015	445	0.22	0.083
CB-03	EBR-II	U-15 Pu-10 Fz	Nb-1 Zr	0.156	0.015	445	0.21	0.080
CB-04	EBR-II	U-15 Pu-10 Fz	Nb-1 Zr	0.156	0.015	445	0.21	0.080
CD-01	EBR-II	U-15 Pu-10 Fz	Nb-1 Zr	0.156	0.009	435	0.20	0.076
CD-02	EBR-II	U-15 Pu-10 Fz	Nb-1 Zr	0.156	0.009	435	0.17	0.065
LA-02	EBR-II	U-15 Pu-10 Fz	Hastelloy-X	0.153	0.011	440	0.19	0.072
PA-01	EBR-II	U-15 Pu-10 Fz	Nb-4 V	0.156	0.009	435	0.19	0.072
C-93	EBR-II	U-20 Pu-10 Fz	Nb-1 Zr	0.156	0.009	430	0.19	0.072
C-97	EBR-II	U-20 Pu-10 Fz	Nb-1 Zr	0.156	0.009	430	0.18	0.068
C-98	EBR-II	U-20 Pu-10 Fz	Nb-1 Zr	0.156	0.009	430	0.17	0.065
C-99	EBR-II	U-20 Pu-10 Fz	Nb-1 Zr	0.156	0.009	430	0.17	0.065
C-100	EBR-II	U-20 Pu-10 Fz	Nb-1 Zr	0.156	0.009	430	0.17	0.065
C-101	EBR-II	U-20 Pu-10 Fz	Nb-1 Zr	0.156	0.009	430	0.18	0.068
CM-01	EBR-II	U-20 Pu-10 Fz	Nb-1 Zr	0.156	0.015	435	0.18	0.068

Capsule CP-40 contained six specimens numbered N-1 through N-6. The specimens were not designed to achieve maximum burnup but instead were designed to test theoretical relationships between fuel volume, void volume, and jacket strength. On these considerations, the specimens were designed to reach only 3.1 a/o burnup. When this burnup was reached all specimens were intact. Irradiation was deliberately continued to determine the jacket failure point. All specimens were still intact at 5 a/o burnup, after which the first evidence of jacket rupture was shown. Neutron radiography at 5.7 a/o burnup disclosed that four of the six specimens had ruptured or deformed jackets, and irradiation has therefore been discontinued. The important conclusions that can be drawn from these results are:

(i) All specimens achieved burnups at least 60% higher than they were designed to reach.

(ii) Two of the specimens did not show jacket rupture after burnups 80% higher than they were designed to achieve.

(iii) The two specimens which did not show jacket failure had a greater ratio of radial expansion to axial expansion than did the others, indicating that radial clearance is more effective than axial clearance in extending fuel burnup.

All other CP-5 specimens examined were found to be intact, except possibly specimen N-10, which showed evidence of jacket deformation. The location and characteristics of the apparent deformation indicate that it is due to a tubing defect.

b. Ceramic Fuel Irradiations. The irradiations currently in progress are summarized in Table XVI. Two forms of mixed carbide are being studied: physical mixtures of powders of UC and PuC, and solid solutions of (U, Pu)C. The physical mixtures are being studied in the form of vibratorily-compacted rods. The solid-solution material is being studied as both vibratorily-compacted rods and sintered pellets. The irradiations in MTR are on specimens approximately 3 in. (8 cm) long in instrumented temperature-controlled capsules. The specimens in EBR-II have a 13 in. (33 cm) fuel length and are located in a special subassembly.

TABLE XVI. Status of Ceramic-fuel Irradiations

Specimen No.	Reactor	Fuel Composition, w/o	Clad Composition, w/o	Clad ID, in.	Clad Thickness, in.	Maximum Clad Surface Temp, °C	Calculated Burnup to Date	
							a/o	(t/cm ²) x 10 ⁻²¹
MV-1	MTR	UC-20 PuC	Nb-1 Zr	0.257	0.012	640	3.0	1.0
MV-2	MTR	UC-20 PuC	Nb-1 Zr	0.257	0.012	640	4.2	1.3
MV-3	MTR	UC-20 PuC	Nb-1 Zr	0.257	0.012	760	4.5	1.7
MV-4	MTR	UC-20 PuC	Nb-1 Zr	0.257	0.012	670	3.5	1.2
MV-5	MTR	UC-20 PuC	Nb-1 Zr	0.257	0.012	760	4.3	1.5
MV-6	MTR	UC-20 PuC	Nb-1 Zr	0.257	0.012	620	4.4	1.6
SMV-2	EBR-II	UC-20 PuC	304 SS	0.257	0.020	600	0.39	0.10
HMV-5	EBR-II	UC-20 PuC	Hastelloy-X	0.267	0.015	600	0.39	0.10
NMV-11	EBR-II	UC-20 PuC	Nb-1 Zr	0.257	0.012	600	0.39	0.10
S-7	MTR	US	Nb-1 Zr	0.257	0.012	550	3.1	0.74
S-8	MTR	US	Nb-1 Zr	0.257	0.012	720	4.7	1.2
S-9	MTR	US	Nb-1 Zr	0.257	0.012	730	4.7	1.2
S-10	MTR	US	Nb-1 Zr	0.257	0.012	710	4.7	1.2
S-11	MTR	US	Nb-1 Zr	0.257	0.012	530	2.5	0.53
S-12	MTR	US	Nb-1 Zr	0.257	0.012	660	3.2	0.76
S-13	MTR	US	Nb-1 Zr	0.257	0.012	680	3.4	0.86
S-14	MTR	US	Nb-1 Zr	0.257	0.012	680	3.7	0.95
S-15	MTR	US	Nb-1 Zr	0.257	0.012	570	2.1	0.39
S-16	MTR	US	Nb-1 Zr	0.257	0.012	650	3.9	0.82
S-17	MTR	US	Nb-1 Zr	0.257	0.012	650	2.7	0.56
S-18	MTR	US	Nb-1 Zr	0.257	0.012	770	4.4	1.1

The uranium sulfide is being irradiated in instrumented temperature-controlled capsules in the MTR. Specimen lengths are approximately 3 in. (8 cm) long.

Measurements of fission gas release have been made of a group of high-burnup vibratorily compacted carbide specimens (see Progress Report for July 1965, ANL-7082, p. 38). The results are shown in

Table XVII. Fission gas release from the hyperstoichiometric carbide was very low, confirming earlier measurements on specimens with lower burnups.

TABLE XVII. Fission Gas Release from Vibratorily Compacted Carbide Specimens

Specimen No.	Fuel Material, w/o	Jacket Material	w/o C in PuC	Burnup, a/o	Max Jacket Surface Temp, °C	Gas Release, % of Theoretical
C-43	PuC	Nb-1 Zr	4.24	5.3	550	31
F-19	UC-20 PuC	304 SS	6.22	5.8	570	<1
F-20	UC-20 PuC	304 SS	4.24	6.8	600	40
C-72	UC-20 PuC	Nb-1 Zr	6.22	6.8	635	<1
C-70	UC-20 PuC	Nb-1 Zr	4.24	6.8	650	20

A capsule containing six carbide specimens has been shipped to the MTR for insertion during the next reactor shutdown. The capsule contains four UC-20 w/o PuC and two PuC specimens. All are vibratorily compacted and all are in Nb-1 w/o Zr alloy jackets. Target jacket surface temperatures and burnups are 1000°C and 2 a/o, respectively.

D. Other Reactor Fuels and Materials Development

1. Nondestructive Testing

a. Determination of Elastic Moduli of High-temperature Materials by Ultrasonics. The sound-velocity data for a tungsten sample at room temperature (see Progress Report for August 1965, ANL-7090, p. 41) have been used with published values of the thermal expansion to make calculations for temperatures up to 900°C.

The rod was mounted in the Brew furnace with the intention of obtaining data for as high a temperature as possible, but inability to properly cool the rod prevented data from being taken at temperatures over 1300°C. Velocities and moduli have been calculated up to this temperature, but corrections due to thermal expansion have not yet been applied for temperatures above 900°C.

b. Ultrasonic Instrument and Transducer Development. Another sample of porous Type 316 stainless steel, according to the manufacturer about 89% dense, was received and evaluated this month. Our measurements show it to be about 79% dense. To obtain this density the manufacturer had to use a smaller particle size than had been used in previous samples. Consequently, measurements of this sample did not fit the curves plotted for the previous samples. However, the acoustic impedance of this sample is close to the impedance of PZT-4 (lead zirconate-titanate) transducers; the sample has an impedance of about 36×10^6 kg/m²-sec, whereas PZT-4 has an impedance of 34×10^6 kg/m²-sec. Tests will be conducted to determine the absorption properties of this sample.

Velocities and densities for several tungsten-loaded epoxies were also determined; the results, as in Table XVIII, show that it is very hard to prepare a mixture having the high acoustic impedance necessary to match PZT-4 transducers.

TABLE XVIII. Data for Tungsten-loaded Epoxies

Density (g/cm ³)	Longitudinal Wave Velocity (10 ⁵ cm/sec)	Acoustic Impedance (10 ⁶ kg/m ² -sec)
1.18	2.66	3.14
1.19	2.08	2.48
2.83	1.63	4.62
4.05	1.33	5.36

c. Development of a Neutron-image-intensification System. Measurements of output phosphor brightness of the second neutron-image-intensifier tube (see Progress Report for September 1965, ANL-7105, p. 48)

have been obtained as a function of neutron intensity. The brightness is a linear function of thermal-neutron intensity over the range from 10^4 to 10^7 neutrons/cm²-sec. The total output brightness of the second tube is appreciably higher than that obtained from the first tube. A value of 28.5 ft-Lamberts (2.65 m-Lamberts) was observed for a thermal-neutron intensity of 2×10^7 n/cm²-sec. This compares with a brightness value of 18 ft-Lamberts (1.67 m-Lamberts) observed with the first intensifier tube under similar conditions. The brightness increase from the second tube is attributed to a more efficient photoemissive layer within the tube.

The anticipated improved resolution capability of the second intensifier tube was experimentally confirmed. A through-hole as small as 0.35 mm in diameter in a cadmium test object was observed, even through the television system. A hole diameter of 0.5 mm was the limiting size which could be observed with the first intensifier tube. The improvement is the result of decreased internal spacing between the intensifier tube window and the input target of the tube.

The neutron transmission of several glass intensifier tube windows was checked by observing the difference in output phosphor brightness of the intensifier tube with and without the extra window in the neutron beam. The differences in transmission for several window types was very small. The flatter window, comparable to the one used on the second intensifier tube, showed slightly improved transmission when compared with the other samples tested.

d. Infrared Systems for Nondestructive Testing. One of the major problems in thermal or infrared testing concerns the emissivity of the surface of the test material. To translate the information derived by thermal measurements, emissivity variations have to be known so that such changes are not misinterpreted as temperature differences. Tests were conducted to compare emissivity effects on InSb radiometer and thermistor systems.

For this test, a steel plate was polished and finished with a flat black paint. The flat black paint was removed from an area 5.08 cm square to reduce the surface emissivity. By scanning through this area of abrupt emissivity change, the effects upon the thermistor system could be compared with the effects on the infrared radiometer.

Traces from the radiometer scan indicated a loss in signal from the polished area. This loss in signal caused by the lower emissivity corresponds to a loss in signal approximately equal to a 6°C temperature difference. The loss in signal caused by the lower emissivity on the thermistor scan was approximately equal to a 1°C temperature difference. Even though the emissivity variations are not as great in the thermistor system, the problem still exists because of the increased sensitivity of the thermal system.

E. Engineering Development

1. Two-phase Flow

a. Void Fraction--Pressure-drop Facility. This experimental facility was designed to investigate the two-phase flow characteristics of boiling sodium; in particular, it was desired to obtain experimental information pertinent to the vapor volume fraction and two-phase frictional losses in an adiabatic system.

This experiment has been terminated except for the possibility that additional stability studies may be run at a later date. A topical report is being prepared.

2. Boiling Liquid-metal Technology

a. Niobium-1% Zirconium Loop. This facility is designed to investigate the heat transfer and two-phase flow characteristics of boiling sodium to a maximum temperature of 2100°F and a maximum pressure of 8 atm. Among the variables to be investigated are (a) boiling heat flux and temperature difference up to occurrence of the critical heat flux, (b) boiling and adiabatic two-phase pressure drop, and (c) vapor volume fraction and boiling stability parameters.

Cleaning and assembly of the loop-support structure is in progress. All stainless steel parts have been cleaned and polished. Portions of the support structure were placed in the vacuum chamber prior to bake-out and pumpdown. These cleaned and polished parts did not affect the minimum chamber pressure or the pumpdown rate, indicating little or no outgassing.

All parts for the thermal radiation-heated boiler and preheat section have been fabricated and are being cleaned prior to final assembly.

The sodium dump tank is complete and has passed the leak-check test. The parts of the argon-purification system have been welded and will be integrated into the sodium-purification sampling systems and the dump-fill tank operation.

Instrumentation systems are nearly complete with the exception of the thermocouple assemblies which have been further delayed by vendor fabrication problems. Another ion gage has been added to the chamber to check the mass-spectrometer readings. The residual-gas analyzer has proven very useful in determining the type and amount of outgassing present during vacuum chamber operation. The pressure transducers have been calibrated and the data fitted by a least-squares method,

yielding an excellent fit with a third-degree polynomial. The diaphragms of the transducers appear to be excellent. The long-term stability of the electronics is not as good as expected. A simple method for calibrating amplifier gain from day-to-day has been worked out.

Orientation of personnel to vacuum-chamber operation is in progress. The empty chamber reached 1×10^{-8} Torr at 70°F and 2.8×10^{-7} Torr at 500°F after $4\frac{1}{2}$ days of operation. The gas analyzer showed that water vapor is the dominant outgassing constituent.

b. Heater Experiments

(i) Electron-bombardment Heater Experiment. The mechanical difficulties previously encountered with insulators and power leads appear to be solved with maximum lead flexibility commensurate with current capacity.

Short-term operation of the heater has revealed a mismatch between the heater circuit and the high-voltage power-supply control. Modifications of the electron heater circuit, the cathode heater circuit, and the control input of the main power supply are in progress. These changes will provide finer control of the cathode temperature and the high-voltage input so that the 10-Amp electron current limit will not be exceeded.

3. General Heat Transfer

a. Countercurrent Turbulent Liquid-metal Flow. Relatively minor revisions of the existing mercury heat exchanger loop--previously used for cocurrent flow experiments--were completed and others are being considered. Emphasis is directed to the use of new experimental techniques related to the generalized mathematical formulation described recently at the Conference on Application of High Temperature Instrumentation to Liquid-metal Experiments held at ANL, Sept 1965.¹⁹ Improvements in test-section design are also being considered.

Exploratory computations (see Progress Report for July 1965, ANL-7082, p. 41) have determined fully developed heat transfer coefficients over wide ranges of operating conditions, but have not been successful for the determination of "Effectiveness Coefficients." A likely cause of the difficulties has been determined and will require a relatively small change in the present computational technique being investigated.

b. Cocurrent Laminar Liquid-metal Flow. Although the required computations related to the general problem of cocurrent laminar flow in a concentric tube exchanger were completed (see Progress Report for July 1965, ANL-7082, p. 42), the original plan to make full use of recently acquired hybrid (analog/digital) computing facilities was not followed. The

¹⁹The proceedings of this conference are to be published as ANL-7100.

Applied Mathematics Division, however, considered the problem of sufficient interest to warrant its use as a demonstration case for the hybrid facility. The facility is now operating satisfactorily and has successfully repeated the previous computations with about a tenfold decrease in overall computing time. The apparent high efficiency of the hybrid computing facility has led to considering its use for countercurrent flow cases.

F. Chemical Separations

1. Fluidization and Volatility Separations Processes

a. Recovery of Uranium and Plutonium from Low-enrichment Fuels: Engineering Work

(i) Engineering-scale Alpha Facility. The ventilation system for the Alpha Facility and the ventilation control units represent the major safety system in the operation of the Facility. A final check of the ventilation and control systems has been made. Leak-testing of the large alpha box containing plutonium-processing equipment was completed. The measured leak rate was 0.11 cfm at 2-in. water pressure; this is equivalent to 0.42% box volume per hour. This leak rate is considered to be satisfactory. Under normal operation the box will be at a negative pressure of 0.5 in. water.

A shakedown test on the converter, simulating the separation of plutonium from UF_6 by thermal decomposition of PuF_6 , was made to demonstrate the operating procedure and equipment flow system. The test involved the transport of a UF_6 (without PuF_6) gas stream, diluted with nitrogen, through the 2-in.-dia converter, which contained 1.5 kg of -100-mesh alumina at 300°C . The UF_6 was collected in a refrigerated condenser downstream of the converter. It is expected that any PuF_6 in the UF_6 gas stream will thermally decompose to solid PuF_4 on the alumina in the converter, and the solid PuF_4 will collect in the fluid bed of alumina particles.

In the shakedown test UF_6 , diluted to 50 v/o by nitrogen, was fed at rates of 15, 20, and 23 g/min to the fluid-bed converter reactor. A total of 7,762 g of UF_6 was processed during the 6.8-hr run period. The superficial gas velocity in the converter was approximately 0.15 ft/sec. Analyses of samples of the alumina bed material after the test indicated that very little uranium (<5 g) had deposited on the bed material. Collection efficiency of the condenser downstream of the converter reactor was very high; only 50 g of UF_6 (out of 7,762 g UF_6 fed) passed through the condenser and was sorbed on a sodium fluoride backup trap.

(ii) Decladding and Fluorination of Uranium Dioxide Fuels. A test with the fluid-bed pilot-plant facility demonstrated decladding of Zircaloy-2-clad uranium dioxide fuel bundles. The facility consisted of a

6-in.-dia fluid-bed reactor, a 9-in.-dia down-flow packed-bed filter, and a 6-in.-dia pyrohydrolysis reactor for the conversion of volatile chlorides to solid oxides. The fuel bundle consisted of 25 Zircaloy-2 tubes, 28 in. long, loaded with a total of 15.8 kg of UO_2 pellets and held in a square array with 0.14-in. spacing between tubes. The wall thickness of the Zircaloy-2 tubes was 0.030 in. The fuel bundle array, immersed in a fluid bed of refractory alumina particles, was contacted with 40 to 85 v/o HCl in nitrogen at bed temperature of 395°C. Progress of the decladding reaction was continuously monitored by hydrogen analyses of the off-gas stream and by gamma-ray photography of the tube bundle. Both techniques indicated that the decladding step was complete in 4.4 hr. The average reaction rate was 0.9 kg Zircaloy-2 per hr, while the HCl utilization efficiency averaged 17%.

Uranium loss by transport with volatile ZrCl_4 through the packed-bed filter was 0.004% of the uranium charged to the reactor. Analyses of the packed-bed filter indicated that both uranium and chloride were not distributed uniformly throughout the filter. Uranium and chloride contents of the upper surface of the filter were 1.9 and 6.1 w/o, respectively, while the respective concentrations of these materials in the bottom layer of the filter were 0.003 and 0.02 w/o.

Further tests will investigate the effect of depth of immersion of the fuel bundles in the fluid bed on the progress of the hydrochlorination reaction.

(iii) Supporting Studies on Fluidization of Fine Particles. In the fluid-bed fluoride volatility processing of UO_2 fuels, several operations are performed in fluid-bed equipment wherein fine particles (<200 mesh) are produced. Elutriation and filter blowback tests are under way to determine operational conditions that will maximize the residence time of fine particles in a fluidized-bed reactor.

A series of tests was performed to measure the elutriation rate of nickel fines (of 19- μ dia) from a fluidized bed of alumina powder (particle size range -80 +170 mesh). The median diameter of the elutriated nickel fines was observed to increase as the elutriation progressed. This is attributed to the initial rapid elutriation rate of the smaller diameter particles in the nickel fines.

In tests in which the concentration of nickel fines in the alumina bed was increased from 4 to 50 w/o, it was observed that the elutriation rate of the nickel fines generally decreased with an increase in fines concentration.

Tests are in progress to determine the conditions that favor removal of material that collects on the surface of sintered metal filters by reverse flow of gas through the filters (blowback of the filters).

G. Sodium Coolant Chemistry

1. Control of Sodium Oxide Impurity

The sodium loop containing the United Nuclear electrochemical cells (see Progress Report for August 1965, ANL-7090, p. 53) has been operating continuously since August 26, 1965. Previous to that time, the cells had been subjected to a one-week run at temperatures ranging from 593 to 610°F. The voltage developed by the cell TP-32 started at 1.272 and dropped to 1.22 V at the end of the week. Cell TP-33 generated 1.214 V at startup and the voltage gradually decreased to a slightly fluctuating 1.19 V. By chemical analysis, the average oxide content of the sodium was 28 ppm at the start of the one week run and 39 ppm at the end of the period.

Since the loop has been running continuously, the temperature of cell 32 has varied between 578 to 600°F while the voltage ranged 1.181 to 1.198 V. The temperature of cell 33 varied between 580 and 607°F with the voltage varying between 1.157 and 1.189 V. The chemical analysis of sodium during mid-September was 37 ppm oxygen. After a short cold-trapping treatment during the first week in October, the oxygen concentration was reduced to 27 ppm. Data for cell behavior with reference to temperature and oxygen content are being correlated. The plugging meter at this time showed an oxygen content of 26-28 ppm.

H. Plutonium Recycle Program

1. Operations

The 22-assembly loading in the EBWR (see Progress Report for September 1965, ANL-7105, p. 58) was rearranged in a more symmetric configuration. For the new configuration, the cold, unpoisoned, reactor was critical with all control rods fully withdrawn except the central rod, which was at a height of 41 in. The reactivity worth of the remaining 7 in. of the central control rod was found to be 10^{-3} from measurement of its differential worth.

2. Reactor Plant Preparation and Maintenance

Safety valves No. 4 and No. 5, which were installed in the 1959 conversion of the EBWR, were refitted with new alloy steel springs for the lowered maximum system pressure of 650 psig. Both valves were re-installed in their positions near the turbine condenser into which their discharges are connected.

Deficiencies in the designs of filters No. 1, 3, and 4 (described in Progress Report for April 1965, ANL-7045, pp. 46-47) were corrected, and these components were returned to the system for further service.

Carbon steel welds between the carbon steel reinforcing rings and the Van Stone-type carbon steel body flanges of filters No. 3 and 4 (described in Progress Report for May 1965, ANL-7046, p. 64) were magnafluxed to assure freedom from cracks. Repairs were not required. Filter No. 2 was scrapped after the salvage of flange parts needed for filter No. 1.

Repair of stainless steel Type 304 piping welds in the 8-in. high-pressure steam line to the Reboiler Plant was resumed. These repairs and radiography were interrupted by the initial approach-to-criticality experiments with plutonium fuel.

III. ADVANCED SYSTEMS RESEARCH AND DEVELOPMENT

A. Argonne Advanced Research Reactor (AARR)

1. General

The architect-engineer has developed five basic arrangements for the AARR plant complex; one has been chosen for intensive further development as the principal Title I design. The scheme differs from the earlier Argonne concept in a number of ways which will improve both operating flexibility and economy of construction. The more important differences are:

- a. removal of the fuel-handling and storage-canal complex from the main reactor containment building;
- b. lowering of the main experimental floor and reactor below grade, and raising of the now adjacent canal complex above grade, to provide identical water levels in the canal and reactor pool;
- c. elimination of one subgrade level in the reactor containment building;
- d. elimination of equipment building and relocation of contents to other areas of the plant complex.

Although the accepted arrangement scheme constitutes a considerable departure from the earlier concept, none of the changes affect the basic design and safety criteria upon which the Preliminary Safety Analysis Report is based.

The architect-engineer has reviewed the PERT/Time logic networks established for the Title I design effort, and has applied management techniques to effect a reduction of about three months in the previously anticipated Title I schedule. The total duration for Title I is now estimated at about eleven months.

The PERT/Cost report on the A-E Title I effort, based on September 1, 1965 information, has been released (see Progress Report for September 1965, ANL-7105, p. 59). This is the first PERT/Cost report to be issued on AARR.

The output included Management Summary, Project Status, Manpower Loading, and Financial Plan and Status Reports in several sorts and at several levels. A study of these reports is currently in progress to designate the report formats which will be most useful to the various interested parties.

In subsequent PERT/Cost updating, the scope of the report will be expanded to include all of the construction phase of the project, and ultimately the R&D effort as well.

2. Theoretical Physics Analyses

The computer program MAC²⁰ has been used for approximate computations of gamma-ray-flux levels in the outer radial reflector of AARR, at the midheight of the active core zone, so that approximate heating rates to be expected in the pressure vessel may be determined.

A subsidiary output was the distributions of neutron fluxes. More sophisticated computations should be made, and will be made, for the absolute magnitudes of the neutron fluxes. Nevertheless, some of the more interesting results on neutron fluxes are summarized here, principally those which relate to comparison of neutron-flux levels when the composition of the radial reflector is changed.

MAC has been reprogrammed at Argonne National Laboratory to solve for neutron-flux distributions in spherical or cylindrical geometry, as well as in slab geometry. The reprogramming has not been extended to solution for the gamma-ray fluxes in other geometries, however, and slab-geometry formulas were retained for the computations of gamma dose rates.

For the neutron fluxes, spherical geometry was selected as the most appropriate one-dimensional model, since the ratio of height to diameter in the reference core is close to unity. The core was chosen to have a volume equal to the total volume of the reference core plus internal thermal column. A given radial cylindrical-annulus region was approximated as a spherical annulus of the same thickness. Each region was uniform in composition, namely, the volume-averaged local composition.

In the reference design core, the power density peaks at the edges of the core. This is a principal feature of the core design, to increase the probability that fission-spectrum neutrons will leak from the core, with resultingly higher useful fluxes of thermal neutrons in the internal and external radial reflectors. For the MAC problems, a constant power density was chosen to reflect approximately the actual nonuniform power distribution.

Four MAC problems were solved. Two problems corresponded to a range of beam-tube voidings of the beryllium and the water between the beryllium and the pressure vessel. The inferred heating rate at the inner surface of the $3\frac{1}{2}$ -in.-thick steel pressure vessel is as high as ~ 0.35 W/g for an actual reactor operating at 240 MWt. The pressure vessel attenuates this exponentially to a heating rate only $1/12$ this high at the outer surface of the vessel. In determining these values, the beam-tube voids were treated as uniform voids in the various reflector regions. Inclusion of a streaming correction would increase the calculated heating rate in the immediate vicinity of the beam tubes and also in the general pressure-vessel region

²⁰Peterson, E. G., MAC - A Bulk Shielding Code, HW-73381 (April 1962).

near beam-tube nozzles. This whole problem is being studied further to check the accuracy of the values of the power density in the pressure vessel.

A significant conclusion is that the heating of the pressure vessel is due almost entirely to capture of gamma rays leaking from the reactor core and from regions between the core and the vessel. Roughly, $3/4$ of these gammas come directly from the reactor core. If necessary, a gamma shield near the inner surface of the vessel could be used to reduce the thermal stresses in the vessel.

The other two MAC problems were related to the possible use of neutron "windows," between the beryllium and the pressure vessel, to increase the level of the thermal-neutron flux beyond the vessel. The goal of this design is to locate instrument tubes, for the nuclear instrumentation, outside the pressure vessel. In one problem, the entire water zone between the beryllium and the vessel was replaced with graphite, canned in aluminum and with $\sim 5\%$ of the volume occupied by coolant water. Beyond the pressure vessel was a water zone 2 ft thick. For the other MAC problem, aluminum, also with 5% water for cooling, was used instead of the graphite.

The calculations indicated that both graphite and aluminum increase the thermal-neutron flux beyond the pressure vessel and also reduce the heating rates in the vessel. In both respects the aluminum is very much more effective than the graphite, reducing the heating rate at the inner surface of the pressure vessel to roughly 0.02 W/g , exclusive of effects of streaming of gamma rays in the beam tubes.

The level of the computed unperturbed thermal-neutron flux in group 31 (0 to 0.076 eV) was $\sim 1.5 \times 10^{10} \text{ n-cm/cm}^3\text{-sec}$ at a distance of $\sim 1\frac{1}{2} \text{ in.}$ from the outer surface of the pressure vessel, at a reactor power of 240 MWt . At greater distances, the computed group-31 neutron flux attenuated rapidly, dropping roughly 50% per inch. Some of this drop-off is due to the superimposed condition that the neutron fluxes vanish at a distance of $2 \text{ ft (H}_2\text{O)}$ beyond the vessel; but this effect is small in the vicinity (2 to 4 in.) of the vessel. However, the introduction of the instrument tubes will depress the thermal-neutron flux. In a practical design, with a coolant passage at the inner surface of the vessel, with aluminum blocks of reasonable size, and with a number of instrument tubes in that region beyond the vessel, it is not clear that a thermal-neutron-flux level as high as 1×10^9 could be attained at 100 MWt . Consideration will be given to a better simulation of the design geometry and region composition in the criticality facility, for additional experimentation on this problem. For example, the $3\frac{1}{2}\text{-in.}$ -thick pressure vessel is a large sink for thermal neutrons, and a local simulation of this steel is important.

3. Heat Transfer

A program is in progress to measure the maximum feasible steady-state power level in a test section simulating AARR Mark-I design (see Progress Report for September 1965, ANL-7105, p. 63). The critical heat flux under various steady flow conditions and also under conditions with a large bypass flow in parallel with the test section will be evaluated.

The valving between the pump and the test section has been rebuilt to extend the obtainable range of flow rates, and the valve portion of the automatic pressure-control system of the loop has been rebuilt. In the flow-rate and pressure ranges of interest, the system now maintains a steady pressure with no "hunting."

Heat balances and adiabatic pressure drops (with both cold and hot inlet water) have been measured across the test section now in the loop.

4. Stress Studies of the Reactor Vessel

A computer program, SEAL-SHELL-2²¹ is now available for the stress analysis of a shell of revolution with axisymmetric pressures, temperatures, and distributed loads. Several changes have been made for use with the Argonne CDC 3600 computer.

The program is based on the finite-element method of calculation, in which a shell is approximated by a series of straight or curved segments. Each segment may have different elastic properties and pressures, and may vary linearly in thickness. Each segment may also have a temperature distribution varying arbitrarily throughout the thickness, but varying linearly along the segment. Since the segments are assumed to be interconnected at the nodal points, the essential elastic characteristics of a segment are represented by the relationship between forces applied to the nodal points and the deflections resulting therefrom. In the SEAL-SHELL-2 program, the force deflection relationship is obtained in the following manner:

- a. For each segment a displacement field is assumed and the strain energy is determined.
- b. By application of the principle of virtual work to the strain energy of each segment, the forces on each segment are determined in terms of deflections. Once the force-deflection relationship is known for each segment, the forces at the nodal points can be computed.

²¹Friedrich, C. M., SEAL-SHELL-2-- A Computer Program for the Stress Analysis of a Thick Shell of Revolution with Axisymmetric Pressure, Temperature, and Distributed Loads, WAPD-TM-398 (Dec 1963).

It should be noted that the approximation in the finite-element method is of a physical nature, i.e., a shell is substituted by a series of straight or curved segments. There need be no approximation in the mathematical analysis of these substitute segments. Also, the finite-element solution will converge to the true solution if the segment size is successively reduced.

Several computations have been made for the AARR pressure vessel. The vessel configuration analyzed is shown in Fig. 20. The shell is divided into 200 segments, the average length of which is approximately 2 in. At the critical regions, the segment size is further reduced to less than 0.5 in. in length, which is far more than necessary for the finite-element method.

The temperature distribution has been computed separately, taking into account variations across the wall thickness as well as along the meridional direction. However, due to the limitation imposed on the SEAL-SHELL-2 program, only 5 points were used to approximate the temperature distribution across the wall thickness. Six stresses, τ_{xy} , S_x , S_θ , S_y , S_{\max} , and $2\tau_{\max}$, were determined at each specified location for each segment, for the following load combinations:

- a. thermal loading;
- b. pressure loading;
- c. boundary effect;
- d. superposition of the above three loadings,

where S_x is the axial stress, S_θ the circumferential stress, S_y the radial stress, S_{\max} the von-Mises generalized stress, and τ_{\max} the maximum shear stress. The maximum stress for the primary and secondary stresses was 34,155 psi, which occurred at the inner surface of the juncture of the spherical shell and the bottom head; this value is slightly greater than the allowable stress. This situation can be easily improved, however, by increasing the inner corner fillet radius. The maximum stress for the combination of primary, secondary, and thermal stresses (see Fig. 20) was 27,534 psi, which occurs at the bottom closure of the vessel.

At the nozzle penetrations, the wall thickness was increased and the primary-plus-secondary stresses were kept around 10,000 psi. It is believed that these nozzles will have a stress concentration factor of 3.5 and that the peak stress will be about 35,000 psi around the nozzle holes. Further study of the peak stresses will be made after the beam-tube arrangement has been finalized.

5. Primary System and Components

The test to determine the corrosion rate of beryllium at 200°F in water flowing at 44 fps has continued (see Progress Report for September 1965, ANL-7105, p. 67). In this test a beryllium surface area

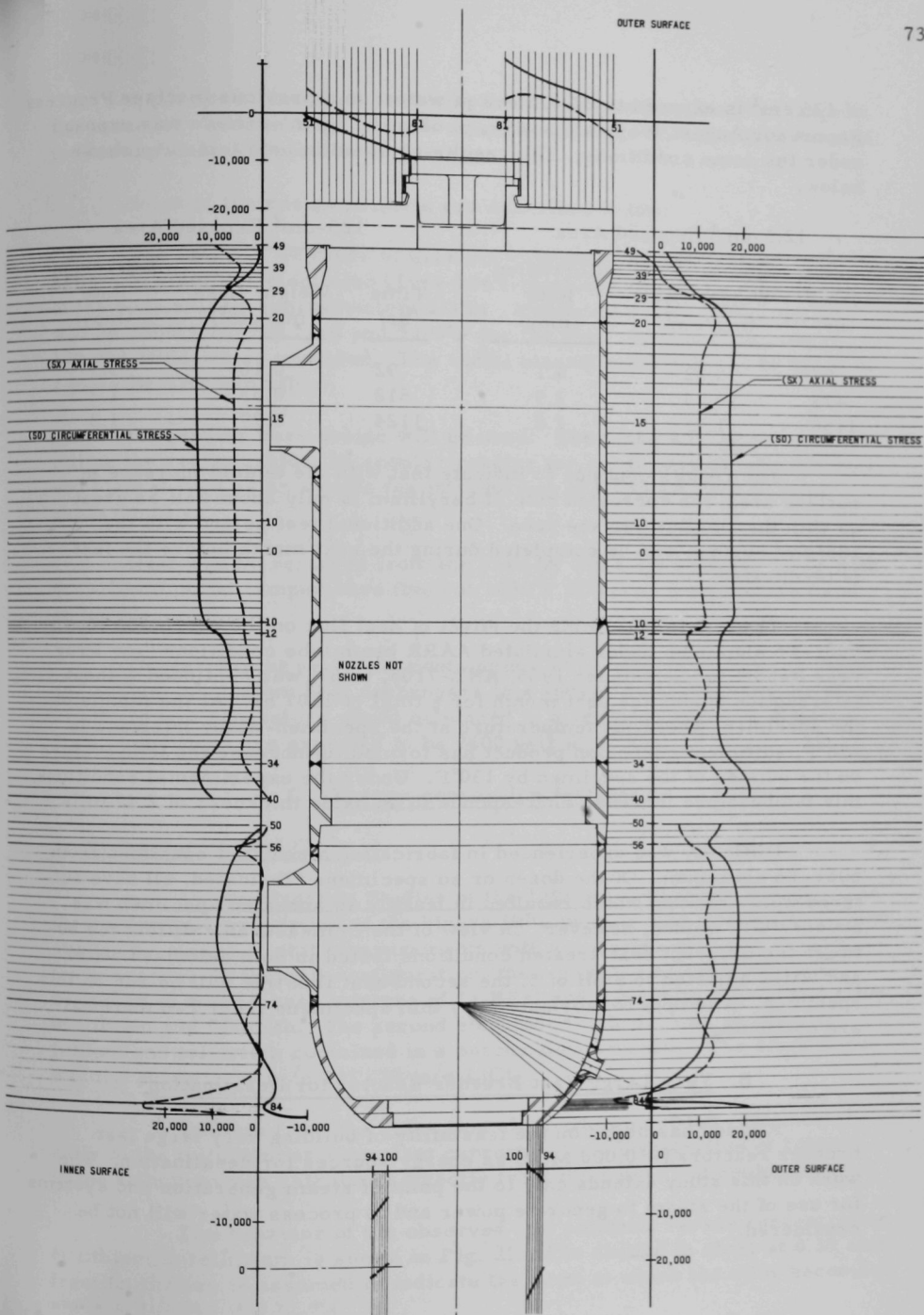


Fig. 20. Primary, Secondary, and Thermal Stresses

of 125 cm² is exposed to 27.6 liters of water; in a previous test (see Progress Report for August 1965, ANL-7090, p. 63) a 12.5-cm² surface was exposed under the same conditions. The results obtained in both tests are shown below.

12.5-cm ² Exposed Area			125-cm ² Exposed Area		
Time (hr)	Weight Loss (mg/cm ²)	Corrosion Rate (mpy)	Time (hr)	Weight Loss (mg/cm ²)	Corrosion Rate (mpy)
97	0.22	4.1	92	0.16	3.3
478	0.75	2.9	518	0.33	1.2
1150	1.75	2.8	1124	0.79	1.3

The results continue to indicate that with the tenfold increase in surface area, the corrosion rate of beryllium is only about half as great as with the smaller surface area. One additional test period with the 125-cm² surface will be completed during the next month before the test is terminated.

The test to determine the effect of heat flux on the corrosion of 6061-T6 aluminum under simulated AARR beam tube conditions (see Progress Report for September 1965, ANL-7105, p. 67) was continued without interruption during the past month for a total of 1507 hr. At the middle of the specimen, where the temperature at the specimen-water interface is 258°F, sufficient corrosion product has formed to increase the temperature on the outside of the specimen by 130°F. Under the experimental conditions, this temperature increase corresponds to an oxide thickness of 2.47 mils.

Difficulty was experienced in fabricating a new test specimen from 6061-T6 aluminum. Of the dozen or so specimens fabricated, all have suffered weld cracking which resulted in leaks. An annealed specimen was successfully welded, however. In view of the immeasurable difference between the different heat-treated conditions tested in both deionized water and water adjusted to a pH of 5, the second heat flux test will be run on this specimen. Attempts to fabricate very thin specimens from T-6 material are continuing.

B. Very Large Fast Breeder Reactor for Desalination

A study has begun on the feasibility of building very large fast breeder reactors (~10,000 MWt) as energy sources for desalination. The work on this study extends only to the point of steam generation and systems for use of the steam to generate power and to process water will not be considered.

A portion of the study involving sodium-to-sodium heat exchangers, the secondary sodium loop, and the steam generators will be subcontracted to Westinghouse Atomic Power Division.

Some of the design criteria are described below:

The fuel will be made of uranium-plutonium carbide bonded with helium to stainless steel clad (Type 304 tentatively selected). The diameter of the rods will be approximately 0.3 in. Maximum design temperatures will be 1300°F for the clad and 3000°F for the fuel. Burnup of at least 100,000 MWd/ton is expected. The radial blanket elements will be made of a metallic uranium alloy.

An annular core design will be used. The fuel-handling scheme will utilize the region inside the annular reactor for decay storage of spent fuel and blanket, and as an avenue for introduction of fresh fuel and blanket subassemblies.

Heat will be removed from the core by using six primary loops with the sodium outlet temperature fixed at 1050°F and inlet temperature fixed at 720°F.

Overall layout envisions containment of the reactor, primary loops, and sodium-to-sodium heat exchangers in a sphere having a diameter of 240 ft. Steam generators would be placed in a separate adjacent building. Steam conditions are expected to be 2400 psig at 900°F.

C. Energy-conversion Systems

1. Regenerative Emf Cells

a. Thermodynamic Studies of the Lithium-Tellurium System. The thermodynamic properties of the binary lithium-tellurium system have been studied by means of emf measurements with a concentration cell without transference. In the cell configuration, the reference electrode (anode) consisted of a two-phase mixture of $\text{Li}_3\text{Bi(s)}$ and a bismuth-rich liquid alloy of lithium and bismuth. The second electrode (cathode) was an alloy of lithium and tellurium contained in a porous BeO crucible. The electrolyte was the eutectic 30 m/o LiF -70 m/o LiCl .

Lithium from the reference electrode was added coulombetrically to the tellurium at a constant current. The concentration of lithium in the tellurium was calculated directly from the number of coulombs used.

The behavior of the observed cell potential versus concentration of lithium in tellurium is shown in Fig. 21. The change in slope at 0.39 atom fraction lithium is assumed to indicate the point at which the alloy becomes saturated with solid Li_2Te .

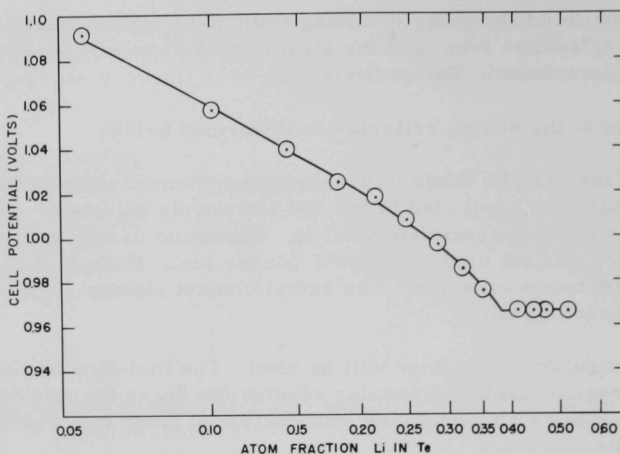
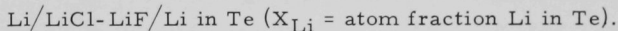


Fig. 21. Voltage-composition Behavior of the Cell:
 $\text{Li} [\text{in Bi}(\ell)]$ saturated with solid Li_3Bi /
 LiCl-LiF/Li in Te (X_{Li} = overall atom
fraction Li in Te) at 798°K

The observed cell potentials were converted (by use of the previously determined²² potential of the reference electrode at 798°K) to those for the cell



The standard states were taken to be $\text{Li}(\ell)$ and $\text{Te}(\ell)$ in the cell environment (saturated with electrolyte). The excess chemical potential of lithium in tellurium, $\Delta\mu_{\text{Li}}^{\text{E}}$, at the cell temperature 798°K was calculated for various atom fractions of lithium in tellurium. From these data, the standard free energy of formation of $\text{Li}_2\text{Te}(\text{s})$ at 798°K was calculated to be -77.9 kcal/mole with an estimated standard deviation of 0.4 kcal/mole .

2. Bimetallic Cells

The physical properties of molten salt electrolytes and molten bimetallic alloys are being measured for use in the engineering design of bimetallic cells and regenerators.

The density, viscosity, and surface tension of the 6.1 w/o NaF-17.7 w/o NaCl-76.2 w/o NaI (15.2 m/o NaF-31.6 m/o NaCl-53.2 m/o NaI) fused salt electrolyte were found to vary as follows with temperature:

²²Foster, M. S., Wood, S. E., and Crouthamel, C. E., *Inorg. Chem.* **3**, 1428 (1964).

Density, 540 to 800°C: $\rho = 3.05 - 0.0009 T$ g/cc;
 Viscosity, 540 to 800°C: $\mu = 3.40 - 0.003 T$ centipoise;
 Surface Tension, 540 to 750°C: $\sigma = 136 - 0.06 T$ dynes/cm,

where T is the temperature in °C.

The densities of liquid sodium-bismuth alloys containing 0, 10.4, 20, 30, 40, and 50 m/o sodium were measured in the temperature range from 300 to 800°C and were found to vary from about 10.1 to 5.3 g/cc.

The densities of liquid sodium-lead alloys containing 0, 10, 20, 30, 41, and 50 m/o sodium were measured at temperatures from 350 to 750°C, and were found to vary from about 10.6 to 5.6 g/cc.

The surface tensions of liquid sodium-bismuth alloys containing 30, 40, 45, and 50 m/o sodium were measured over the temperature interval 400 to 700°C. Over this range of composition and temperature, the surface tensions showed little variation (242 to 260 dynes/cm).

IV. NUCLEAR SAFETY

A. Reactor Kinetics

1. MTR Irradiations of UO₂ Specimens

Ten irradiation capsules, each containing two steel-clad UO₂ fuel pins have been under irradiation in the Materials Testing Reactor in preparation for fast reactor safety experiments to study the effects of prior irradiation on meltdown of oxide fast reactor fuel (see Progress Report for April 1965, ANL-7045, p. 65). The first of three capsules have been removed from the testing reactor and are now cooling, in preparation for disassembly of the irradiation capsules and counting of the Al-0.1 w/o Co flux monitors.

2. Fast Reactor Safety

a. Coolant (Water) Expulsion Studies. Following damage to the thin-wall heated section used in the water-expulsion studies, a new tube was installed. Two runs (to determine the effects of vibration induced by the circuit breaker) were completed, after which the recording oscillograph failed to function. After repairing the oscillograph and after a general delay due to building maintenance, six more runs were completed to investigate the effectiveness of the synchronization system between the motion pictures and the power pulse.

b. Critical Flow Studies. Calculations of the progression of accidents in sodium-cooled reactors reveal that critical flow may exist in the core, leading to detrimental effects such as voidage of the coolant channel, shock-phenomena and pressure buildup.

Figure 22 illustrates calculated sonic velocities for two-phase sodium mixtures. The metastable and equilibrium models represent upper and lower limits on the critical velocities. At 15 psia, the equilibrium sonic velocity is as low as 5 ft/sec. Based on the equilibrium sonic velocity, the occurrence of shocks are possible the instant that vapor is produced in the coolant channel. Similarly, if one considers the metastable sonic velocity and assumes an initial subcooled coolant velocity of 40 ft/sec, the choking phenomenon may be reached at 50% void. The occurrence of shocks will lead to subsonic system velocities, i.e., the expulsion velocity of the sodium is dictated by the critical velocity, or the maximum critical flow rate.

The above illustrations clearly indicate the need for detailed investigations of the critical flow phenomenon in two-phase mixtures in order to describe accurately the expulsion of coolant in a reactor channel.

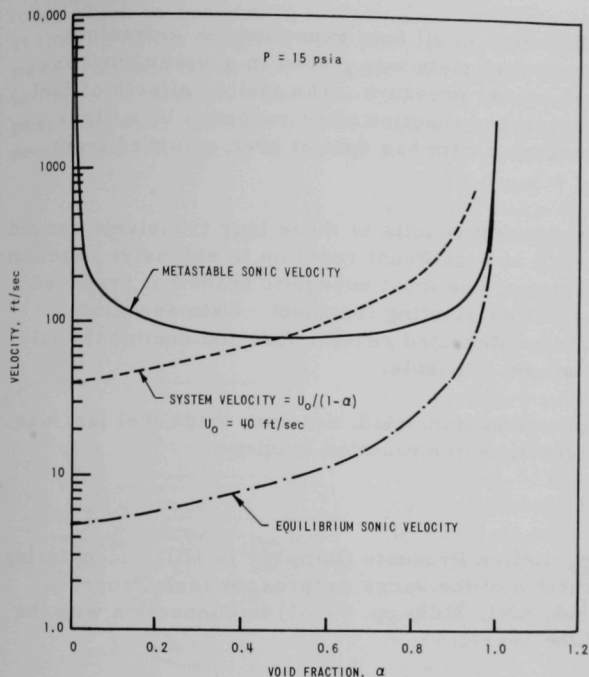


Fig. 22
Sonic Velocities in Two-phase
Sodium Systems

At the present time, experiments are in the design and construction stages to study critical flow of different fluids. The critical flow of sodium will be studied in a number of flow-duct geometries in the pressure range from 1 to 15 psia. Concurrently, an identical experiment with water will be carried out in order to make direct comparisons between the two working fluids.

In addition, detailed measurements of the fluid behavior at the point of choking in rectangular and round ducts are in progress using steam-water mixtures (see Progress Report for August 1965, ANL-7090, p. 73). The overall objectives of these experiments are to obtain methods for interpreting critical velocities, metastability and superheat, velocity ratios, and flow structures in high velocity two-phase flow systems for different fluids.

B. TREAT

1. Operations

Four incremental transients were run on the metal-water transparent series of experiments being jointly conducted by TREAT and the

Chemical Engineering Division. In all four experiments, a uranium-aluminum alloy SPERT-type fuel plate was placed in a water environment at ambient temperature and pressure. The visible effects of fuel plate heating and the metal-water reaction were recorded by a high-speed camera, but the developed film has not yet been returned from the processor.

The immediately apparent results of these four transients ranged from fuel-plate melting with no significant reaction to extensive reaction and fragmentation of the plate. The most energetic transient produced one relatively large resolidified, floating fragment. Data associated with the experiment, such as integrated reactor flux and chemical analysis of the residue, are not yet available.

One CEN capsule, a zirconium-clad, uranium oxide fuel pin, was irradiated as part of the metal-water reaction studies.

2. Large TREAT Loop

a. Construction. Keller Products Company is still encountering difficulties in the construction of the surge suppressor (see Progress Report for September 1965, ANL-7105, pp. 80-81) in connection with the circumferential weld on the vessel.

The major components of the gas system have been tested for operation and helium leak-tightness. Steam leakage was observed in two of the four manually operated, one-inch stainless steel ball valves and in one of the two electrically operated, one-inch stainless steel ball valves. The other electric-operator equipped valve was found to leak significantly through the seat. A seat leakage rate of $0.1 \text{ cm}^3/\text{sec}$ for both helium and air was determined. During preliminary testing, one of the electric operators became inoperative and was removed from the valve in order to complete the leak testing of the valve seat and stem. The faulty valves have subsequently been returned to the manufacturer for inspection and repair.

b. Instrumentation. Adequate instrumentation of the test section of the large TREAT sodium loop requires the measurement of inlet and outlet pressures and of transient pressure pulses generated in the flowing sodium during meltdown experiments. The inlet pressure can be obtained by a direct tap through the heavy-walled pressure vessel into the entry plenum of the fuel section, but pressure measurement at the fuel-section midpoint and outlet is difficult because of the three concentric shells comprising the test section.

The experimental fuel subassembly is supported by a hemispherical mechanical seal located within the bottom of an inner flow

tube, which is suspended from hanger brackets in the header-flow separator at the top of the single-ended pressure tube. The liquid metal flows downward from the header in the annulus between flow tube and pressure tube to the inlet plenum, where the direction of flow reverses and the sodium passes upward through the fuel subassembly within the flow tube. The test section was designed to permit convenient insertion and removal from the TREAT reactor, and to reduce the extreme stresses from differential thermal expansions and mechanical restraint.

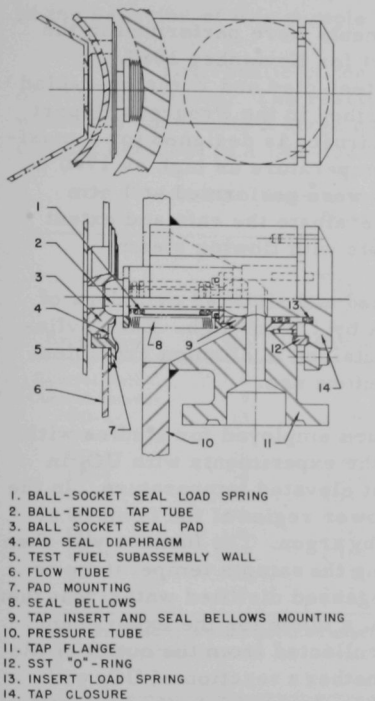


Fig. 23. Design Details of Pressure Tap Used in Large TREAT Sodium Loop

A pressure tap was devised to couple a miniature pressure transducer to the interior of the test fuel subassembly. Figure 23 shows the pressure transducer tap arrangement for penetrating through the pressure tube into the test fuel subassembly. The tap subassembly is mounted on the test-section pressure tube. A spring-loaded bellows-sealed insert (the ball-ended tap tube) extends inside the pressure tube and engages a matching seal pad in the wall of the flow tube. An access hole in the test fuel subassembly lines up with the openings in the tap and seal pad to complete the access circuit. Two such taps are specified for each test section: one each for the midplane pressure tap station and for the test-section outlet station.

With this arrangement, some leakage can occur between the downward flowing sodium in the flow tube and the upward flowing sodium in the test fuel subassembly. Tests were performed in the temperature range 400-500°C, and at pressure differentials up to 2.7 atm. This device is designed to accommodate minor misalignments due to differential thermal expansion. Leak rates were checked for

small vertical displacements of tap and pad. Under design conditions, leak rates around the tap tube are insignificant.

C. Chemical and Associated Energy-transfer Problems in Reactor Safety

1. Metal-Water Reactions

a. UO₂-Steam Reaction. The finding of a significant reaction between UO₂ and water (see Progress Report for October 1964, ANL-6965, pp. 92-93) has prompted the study of the behavior of UO₂ in flowing steam

under isothermal conditions. In the previous studies, unclad UO_2 specimens were exposed to transient neutron bursts in TREAT while submerged in water at room temperature. Three experiments were performed in which the fission energy input was 223, 409, and 775 cal/g; the corresponding quantities of hydrogen generated were 5.7, 17.7, and 16.9 ml (STP)/g UO_2 . The hydrogen evolution was equivalent to the conversion of $\text{UO}_{2.0}$ to $\text{UO}_{2.07}$, $\text{UO}_{2.20}$, and $\text{UO}_{2.19}$, respectively.

The current isothermal experiments were performed in the high-pressure furnace (see Progress Report for November 1964, ANL-6977, p. 82). (Studies with stainless steel-clad and Zircaloy-2-clad UO_2 fuel elements in the furnace were described in the Progress Report for July 1965, ANL-7082, pp. 67-73.) The furnace is designed for a maximum pressure of 1000 psig and a sample temperature as high as 1700°C. The experiments with unclad UO_2 , however, were performed at 1 atm pressure and 1500°C, and were designed to evaluate the rate and extent of reaction of typical high-density UO_2 pellets with flowing steam.

The samples consisted of pressed and sintered cylinders of UO_2 (>95% theoretical density), 1/2 in. in dia by 1/2 in. high. Each cylinder weighed about 19.2 g. The samples, contained in alumina crucibles, were washed and dried to constant weight before use.

The usual experimental procedure employed for studies with the high-pressure furnace was altered for the experiments with UO_2 in order to avoid contact between UO_2 and air at elevated temperature. In the experiments, the UO_2 was inserted into the lower region of the furnace at room temperature and the air was replaced by argon. The furnace was then raised to the operating temperature, bringing the sample temperature to about 650°C. Steam flow, generated from degassed distilled water, was then started. After steam had replaced the argon, a blank for the experiment was obtained, i.e., noncondensable gas was collected from the outlet of the furnace for a period of time to determine whether a reaction of UO_2 with steam occurred at 650°C. The sample was then elevated into the hottest portion of the furnace (1500°C). When the sample temperature reached 1500°C, collection of a second gas sample was begun. The UO_2 sample was held at 1500°C for a predetermined period of time, and was then lowered to its original position. Gas collection was continued for an additional 30 min.

The amount of oxidation was determined by four independent methods: sample weight gain during an experiment, gravimetric analysis (subsequent controlled oxidation of sample residues to U_3O_8), X-ray diffraction, and hydrogen evolution. In the latter technique, the two gas samples described above were analyzed by means of a mass spectrometer. After making a correction for the hydrogen produced by the decomposition of water, the amount of hydrogen evolved from the UO_2 -steam reaction was calculated. Analyses of the "blank" gas samples indicated that no reaction occurred while the samples were at the 650°C position in the furnace.

The atomic ratios of oxygen to uranium were calculated from the results of each of the four methods of analysis (see Table XIX). Good agreement between the methods was obtained. A plot of the final composition (O/U ratio), taken from the weight gain data, as a function of the square root of time is shown in Fig. 24. The reaction rate follows an apparent parabolic law for the first 70 min and then tapers off at a final composition of about $\text{UO}_{2.17}$. In one experiment the pressed-and-sintered UO_2 pellet was crushed to powder before exposure to steam. No difference in the behavior of this sample was noted.

The results of the isothermal experiments confirm the reaction of UO_2 with steam. The reaction is relatively slow at 1500°C and probably would not contribute a large quantity of hydrogen following a loss-of-coolant accident in a UO_2 -fueled power reactor.

TABLE XIX. Oxygen-to-Uranium Ratios of UO_2 Samples before and after Exposure to Steam at 1500°C

Experiment	Time, min	Observed Atomic Ratio of Oxygen to Uranium				
		By Weight-gain Method	By Gravimetric Analysis	By H_2 Evolution	By X-ray Diffraction	
					Major	Minor
Control Pellet	0	-	2.008	-	2.01	-
Control Powder	0	-	2.010	-	2.01	-
UO-6	15	2.076	2.069	-		
UO-7	15	2.075	2.066	2.060		
UO-3	30	2.106	2.102	2.091		
UO-4	30	2.106	2.106	2.088		
UO-1	70	2.149	2.148	2.121	2.01	2.22
UO-5	70	2.142	2.138	2.126		
UO-2 ^a	120	2.159	2.161	2.110	2.24	2.01
UO-8	120	2.158	- ^b	2.146		
UO-9	240	2.170	- ^b	2.160		
UO-10	240	2.173	- ^b	2.184		

^aPellet crushed to powder prior to experiment.

^bResults not yet available.

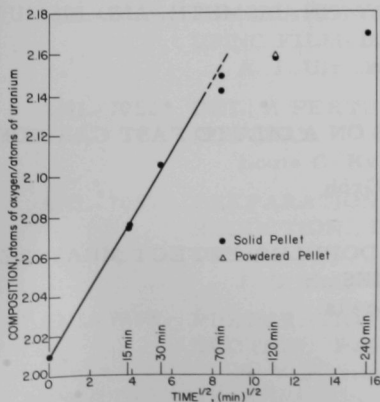


Fig. 24

Oxygen-to-Uranium Ratio after Exposure of UO_2 to Steam at 1500°C and 1 atmosphere Pressure

V. PUBLICATIONS

Papers

AN EXTENSION OF THE FINITE HANKEL TRANSFORM AND APPLICATIONS

Gabriel Cinelli

Intern. J. Eng. Sci. 3, 539-559 (1965)

HEAT TRANSFER IN TWO-PHASE FLOW OF GAS-LIQUID MIXTURES

A. A. Kudirka, R. J. Grosh, and P. W. McFadden

Ind. Eng. Chem. Fundamentals 4, 339-344 (August 1965)

TRANSIENT MAGNETOHYDRODYNAMIC FLOW AND HEAT TRANSFER

R. M. Singer

Z. angew. Math. Phys. 16(4), 483-494 (1965)

ELECTRON EXCITATION OF ZnS(Ag)

Alexander DeVolpi and K. G. Porges

Nucl. Instr. Methods 36(2), 354 (October 1965) Letter

ERRATUM FOR M. ABRAMOWITZ AND I. A. STEGUN, HANDBOOK OF MATHEMATICAL FUNCTIONS, NATL. BUR. STDS. APPL. MATH. SER. NO. 55, FORMULA 4.5.64

H. C. Thacher

Math. Computation 19, 705 (October 1965)

The following appeared in Trans. Am. Nucl. Soc. 8(2), November 1965, as Abstracts:

FLUORINATION OF UO_2 - PuO_2 -FISSION PRODUCT OXIDE PELLETS IN A FLUIDIZED-BED REACTOR

L. J. Anastasia, P. G. Alfredson, and M. J. Steindler

p. 357

STATIC AND DYNAMIC CORROSION BY TIN, BISMUTH, AND BISMUTH-SODIUM ALLOY AT UP TO 1000°C

Hiroshi Shimotake and J. C. Hesson

p. 413

DOPPLER-EFFECT MEASUREMENTS ON A DILUTE FAST CARBIDE ASSEMBLY, ZPR-6 ASSEMBLY 4Z

C. E. Till, R. A. Lewis, and E. F. Groh

p. 454

EQUIPMENT AND TECHNIQUES FOR DOPPLER-EFFECT MEASUREMENT ON FAST CRITICAL ASSEMBLIES

C. E. Till, E. F. Groh, and R. A. Lewis

p. 455

INITIAL USAGE OF A COMPUTER FOR ON-LINE DATA REDUCTION IN REACTOR PHYSICS EXPERIMENTS

C. E. Cohn

p. 585

FLUID-BED FLUORIDE VOLATILITY PROCESSING OF IRRADIATED FUELS IN A HOT CELL

A. A. Chilenskas, K. S. Turner, J. T. Holmes, J. E. Kincinas, and

G. L. Potts

p. 615

INERT ATMOSPHERE ENCLOSURE FOR ENVIRONMENTAL TESTING

J. O. Ludlow, L. F. Coleman, R. F. Malecha, J. H. Schraidt, and

M. A. Slawecki

p. 627

ANL Reports

- ANL-6925 CHEMICAL ENGINEERING DIVISION SEMIANNUAL
REPORT, July-December 1964
- ANL-6929 SAFETY ANALYSIS REPORT FOR THE ARGONNE AD-
VANCED RESEARCH REACTOR CRITICAL EXPERIMENT
C. N. Kelber, E. F. Groh, and K. E. Plumlee
- ANL-7030 OPTIMUM DESIGN OF HIGH-PRESSURE, LARGE-
DIAMETER, DIRECT-NUCLEAR-PUMPED, GAS LASERS
James A. DeShong, Jr.
- ANL-7034 THE RATIO OF U^{238} CAPTURE AND U^{235} FISSION CROSS
SECTIONS IN FAST REACTORS*
William G. Davey
- ANL-7038 A LIQUID-METAL HEAT-TRANSFER EXPERIMENT
R. E. Holtz
- ANL-7039 EVALUATION OF A THERMIONIC ENERGY CONVERTER
USING FILM-BOILING LIQUID METAL
A. J. Ulrich
- ANL-7052 DEL, A PERTURBATION PROGRAM WRITTEN IN
FORTRAN
Louis C. Kvitek
- ANL-7057 PREPARATION OF METALS BY MAGNESIUM-ZINC
REDUCTION. PART I. REDUCTION OF URANIUM
OXIDES
J. B. Knighton and R. K. Steunenberg
- ANL-7058 PREPARATION OF METALS BY MAGNESIUM-ZINC RE-
DUCTION. PART II. REDUCTION OF THORIUM DIOXIDE
A. V. Hariharan, J. B. Knighton, and R. K. Steunenberg

ANL-7059 PREPARATION OF METALS BY MAGNESIUM-ZINC
REDUCTION. PART III. REDUCTION OF PLUTONIUM
DIOXIDE

J. B. Knighton and R. K. Steunenberg

ANL-7106 FARET CORE I FUEL IRRADIATION PROGRAM AND
REFERENCE DESIGN

P. J. Persiani, T. R. Bump, and W. J. Kann

ARGONNE NATIONAL LAB WEST



3 4444 00007812 1